Spring 2018

Investigating the effect of fluid shear stress on the failure of cancer cell membranes: an experimental and computational analysis

Leah M. VanDenBosch
University of Iowa

INVESTIGATING THE EFFECT OF FLUID SHEAR STRESS ON THE FAILURE OF CANCER CELL MEMBRANES: AN EXPERIMENTAL AND COMPUTATIONAL ANALYSIS

by

Leah M. VanDenBosch

A thesis submitted in partial fulfillment
of the requirements for the Master of Science
degree in Biomedical Engineering in the
Graduate College of
The University of Iowa

May 2018

Thesis Supervisor: Associate Professor Sarah C. Vigmostad

Graduate College
The University of Iowa
Iowa City, Iowa

CERTIFICATE OF APPROVAL

_____

MASTER'S THESIS

_____

This is to certify that the Master's thesis of

Leah M. VanDenBosch

has been approved by the Examining Committee for
the thesis requirement for the Master of Science degree
in Biomedical Engineering at the May 2018 graduation.

Thesis Committee: _____
Sarah C. Vigmostad, Thesis Supervisor

_____
Michael D. Henry

_____
Jia Lu

_____
James A. Ankrum

_____
Seth I. Dillard

ACKNOWLEDGEMENTS

There is a plethora of people who have impacted and influenced my personal and academic life. I can acknowledge many people generally and a few specifically, but I hope each person knows how much I appreciate them.

My family and friends have been a constant source of support, providing kind encouragement, therapeutic laughter, much-needed distractions from work, and patient understanding when I needed to put my work before them. My sanity would not have survived without them.

Dr. Sarah Vigmostad, my research advisor, has been a valuable source of opportunity, experience, wisdom, and guidance through both my undergraduate and graduate studies. My gratitude to her for her commitment and encouragement cannot be overstated.

I would also like to acknowledge Dr. Jia Lu, who co-mentored the computational modeling aspect of the project; my other thesis committee members, for their advice and support; and Ben Krog and Devon Moose, who trained me in various experimental procedures and provided me with cell cultures.

It truly takes an entire community to allow the success of one person. If I have advanced science at all, it was not through any extraordinary ability of mine, but through the contributive efforts of an enormous scientific and social community. I am thankful for them all.

ABSTRACT

Cancer metastasis, or the formation of a secondary tumor at a site distant from the primary tumor, is known to be an inefficient process. Historically, it was believed that the shear stresses and forces experienced by cancer cells traveling through the circulatory system are major limiting factors to their metastatic potential and viability. High levels of fluid shear stress are known to be capable of destroying tumor cells. However, more recent research has shown that cancer cells survive migration through the circulatory system and extravasation into distant tissues with a high degree of efficiency, indicating that hemodynamic forces are not primarily responsible for metastatic cancer cell death. A current subject of investigation is the biomechanical effect of fluid shear stress on cancer cells – how do cancer cells react to the fluidic forces and stresses they experience in circulation? This study focused on quantifying the elastic modulus and rupture behavior of prostate cancer and prostate epithelial cells, with and without exposure to fluid shear stress. Micropipette aspiration was the means of inducing deformation and rupture of the cell membrane. Images obtained through micropipette aspiration were analyzed to calculate elastic modulus and to quantify local stresses along the aspirated cell membrane. An axisymmetric stress model of the aspirated cell membrane was solved using MATLAB; the trends for direction and relative magnitude of stresses were confirmed by an Abaqus finite element model.

Results of the micropipette aspiration included statistically significant differences in elastic modulus and rupture pressure between experimental groups. The elastic modulus of epithelial cells exposed to shear stress was significantly higher than that of the cancer cell groups, both exposed and unexposed to shear stress. There was no difference in elastic modulus between cancer cells exposed to shear stress and unexposed to shear stress. This is contrary to the findings of a previous study; prostate cancer cells have been observed to stiffen after exposure to shear stress. It has also been well documented that epithelial cells exhibit higher elastic moduli than

cancer cells; however, no difference was observed in this study in the comparison of elastic moduli of cancer and epithelial cells that were unexposed to shear stress. The rupture pressure of the cancer cells unexposed to shear stress was significantly lower than any other group. This suggests a strengthening reaction of the cancer cell membrane in response to shear stress exposure. This effect was observed to be transient; the increase in rupture pressure disappeared by an hour after the shear stress exposure. The epithelial cells did not exhibit any change in rupture pressure after exposure to shear stress. There was no correlation between elastic modulus and rupture pressure; the stiffness of the cells did not indicate how likely they were to rupture.

The MATLAB and Abaqus models agreed well for trends of principal stresses and von Mises stress. The MATLAB model was quite sensitive to the curvature of the spline fitted to the membrane edge, resulting in irregular patterns and some extreme values of stress and making the results difficult to interpret. The maximum stress did tend to increase with increased aspiration pressure. The location of the maximum stress along the membrane did not reliably correspond to the location of rupture during micropipette aspiration. This model may be improved by automating the process of fitting a spline to the edge of the membrane to reduce user error in plotting individual points.

Further studies to characterize the effects of fluid shear stress on cancer cell mechanics will be useful to confirm differences in elastic modulus and rupture pressure and to investigate the effect of time, temperature, cancer cell line, culture medium, and other variables on cancer cell properties.

PUBLIC ABSTRACT

Cancer cells experience unique fluidic stresses and forces while traveling through the bloodstream during metastasis. Recent research has shown that these forces do not play a major role in metastatic inefficiency, but that cancer cells navigate the circulatory system and extravasate into distant tissue with a high rate of survival. It has also been demonstrated that cancer cells exposed to fluid shear stress exhibit a change in mechanical properties such as the elastic modulus. This study used micropipette aspiration to investigate the effect of fluid shear stress exposure on the elastic modulus and rupture pressure of prostate cancer and epithelial cells. Cancer cell rupture behavior is a relatively new area of investigation, and was quantified in this study by the aspiration pressure at which the membrane ruptures. A computational model was also constructed to quantify local stresses along the membrane of the cell undergoing micropipette aspiration.

The results of the study partially agree with previously published data; the cancer cells exhibited an adaptive response to the fluid shear stress by an increase in their rupture pressure. However, the increased stiffness of cancer cells after exposure to shear stress seen in other studies was not detected in this investigation. It may be concluded that cancer cells react to shear stress by strengthening their membranes in a way that does not increase their stiffness, while epithelial cells do not exhibit any significant reaction to shear stress in either stiffness or failure strength.

TABLE OF CONTENTS

LIST OF TABLES

LIST OF FIGURES

CHAPTER 1: INTRODUCTION

1.1 Background in Cancer Cell Mechanics

Cancer is an often-deadly disease affecting hundreds of thousands of people per year in the United States alone. Some of the most common cancer sites include the lung, breast, prostate, and colon, for a combined incidence rate of 339 per 100,000 people and combined mortality rate of about 100 per 100,000 people (*United States Cancer Statistics: 1999-2014 Incidence and Mortality Web-based Report*, 2017). The mortality rate is much higher when considering global cancer trends; the World Health Organization estimates that one in six deaths is attributable to cancer worldwide (WHO, 2018). Cancer has many causes and risk factors, including obesity, tobacco use, alcohol abuse, poor diet, low physical activity, exposure to asbestos, exposure to radiation, HPV or HIV infection, genetic predisposition (family history), and aging (Forouzanfar et al., 2016). The mechanism of cancer development is the accumulation of DNA mutations due to these risk factors; the mutations alter the cell's normal processes of growth, replication, and death. Cancer cells do not self-destruct when they get old and damaged, as a normal cell would. Instead, they replicate faster than normal and stay alive longer, creating a mass of cancer tissue called a malignant tumor. Tumors can avoid detection and destruction by the immune system, induce blood vessel growth to meet their metabolic needs, and spread to other tissues and organs in the body. Cancer metastasis is the process of cancer cells migrating to other areas of the body and creating new tumors; this advanced stage is referred to as stage four cancer and is often fatal.

Cancer cells typically migrate through the vascular and lymphatic systems. Although a huge quantity of cells may be released into these channels daily, only a tiny fraction of them successfully form a secondary tumor (Fidler, 1970; Luzzi et al., 1998). One historical theory postulated that metastatic inefficiency is due to the destruction of cancer cells by the hemodynamic forces they experience as they travel through the circulatory system (Weiss, Orr, & Honn, 1989). This hypothesis has been challenged by more recent research. One mechanism of

the proposed hemodynamic destruction is the pressure gradient across a cell when it is wedged into a capillary smaller than the cell's diameter (Weiss, Dimitrov, & Angelova, 1985). The occlusion of blood flow in the capillary increases the pressure gradient across the cell, potentially leading to membrane failure. This hypothesis seems unlikely; micropipette and microfluidic experiments can apply high pressure gradients across cancer cells without causing membrane failure (Chivukula et al., 2015). The highly parallel nature of capillary beds is also a protection against large pressure buildup due to occlusion. Another proposed mechanism of destruction is the fluid shear stress imposed on the cancer cell as it traverses the bloodstream (Regmi, Fu, & Luo, 2017). In this study by Regmi, breast cancer cells were subjected to shear stress in a microfluidic system. The lowest level of applied shear stress reported in the study was a normal value for a human artery at rest. The cells experienced continuous shear stress for a minimum of two hours before being tested for viability. The findings were that high levels of shear stress for prolonged periods of time can destroy cancer cells. However, the test conditions applied significantly higher stresses for a much longer time than cells are likely to experience *in vivo*. For the lowest shear and time exposure group, about 90% of injected cells remained viable.

Recent research has found evidence that cancer cells are not as susceptible to hemodynamic destruction as previously thought. Studies by Barnes and Mitchell found that cancer cells are more resistant to destruction by fluid shear stress than normal cells (Barnes, Nauseef, & Henry, 2012; Mitchell et al., 2015). Both studies briefly exposed cancer cells to high levels of fluid shear stress and measured percent viability. Both found that, though a significant amount of cell death occurred from the shear stress exposure, cancer cells had significantly higher viability after exposure than epithelial cells, potentially indicating a protective mechanism. Other groups have challenged the hemodynamic destruction theory and concluded that cancer cell survival during flow through the circulation and extravasation into a distant tissue is remarkably efficient (Chambers, Naumov, Vantyghem, & Tuck, 2000; MacDonald, Groom, & Chambers,

2002). This group used real-time microscopy observation to study cell survival and metastasis efficiency after injection of murine melanoma cells into the vasculature of chick embryos or mice (Cameron et al., 2000; Koop et al., 1995; Luzzi et al., 1998). The studies concluded that only about 10-15% of cells were lost in the microcirculation; the remaining cells successfully migrated out of the bloodstream, though only a small percentage of cells formed metastases. This indicates that cell survival and growth after extravasation are greater contributors to the inefficiency of the metastatic process than hemodynamic destruction.

It has been clearly shown that high levels of fluid shear stress are capable of destroying cancer cells, but it has not been demonstrated that this plays a significant role in limiting the rate of metastasis in the human body. We do know that cancer cells do not respond to shear stress the same way that non-cancerous cells do. It has already been discussed that cancer cells have higher viability rates after fluid shear stress exposure. It has also been shown that cancer cells exhibit different mechanical properties compared to non-cancerous cells before and after exposure to shear stress (Chivukula et al., 2015). Before exposure to shear stress, the elastic modulus of epithelial cells in this study was about 2.4 times that of the cancer cells. The elastic modulus of the cancer cells increased significantly after exposure to shear stress, while the epithelial cells' elastic modulus remained unchanged. These findings suggest that cancer cells have an adaptive response to fluid shear stress, which may protect them against hemodynamic destruction.

An enormous amount of resources is poured into research of the mechanical properties of cancer cells compared to their normal counterparts, including elastic modulus, cortical tension, deformability, viscosity, relaxation, and adhesion. It is hoped that knowledge of these properties will be useful in the identification and treatment of the disease. The effect of fluid shear stress on these mechanical properties is just beginning to be uncovered. However, very little research has been done to investigate the failure strength of cancer cell membranes. Are the pressures and stresses experienced in the circulatory system enough to rupture the cells? Does the increased

stiffness after shear stress exposure demonstrated by Chivukula indicate that cancer cells are less likely to rupture after shear exposure (Chivukula et al., 2015)? Does membrane rupture correlate with a high localized membrane tension?

The goal of this study is to explore these questions. Micropipette aspiration experiments were employed to mechanically deform cells to a rupture point, with and without exposure to fluid shear stress. Cancerous and epithelial prostate cells were used in the experiments. Computational models were built to characterize local stresses in the aspirated membrane. Outcome variables included rupture pressure, elastic modulus, and membrane stress.

1.2 Cell Characterization Techniques

Mechanical properties of individual cells, such as elastic modulus, deformability, cortical tension, and viscoelasticity, may be characterized by several cell manipulation techniques. Among the most widely used are atomic force microscopy, optical tweezers, deformability cytometry, and micropipette aspiration.

Atomic force microscopy measures the deformability of a cell by applying an indentation force to the membrane. A cantilever with a blunt probing tip applies a point force to the cell, while a laser focused on the end of the cantilever is reflected onto a photodetector. Vertical displacement of the cantilever is captured by the deflection of the laser beam, creating measurable photocurrents in the detector (Lekka, 2016). The arrangement is illustrated in Figure 1. The indentation force F between the sample and the probing tip can be calculated by Hooke's law:

$$F = k_C D_C \qquad (1)$$

where k_C is the spring constant of the cantilever and D_C is the vertical displacement of the cantilever. If the stiffness of the tip is much larger than that of the sample, the deformation of the tip can be assumed to be negligible, and the elastic modulus of the sample, E_s, is related to its stiffness by the following equation:

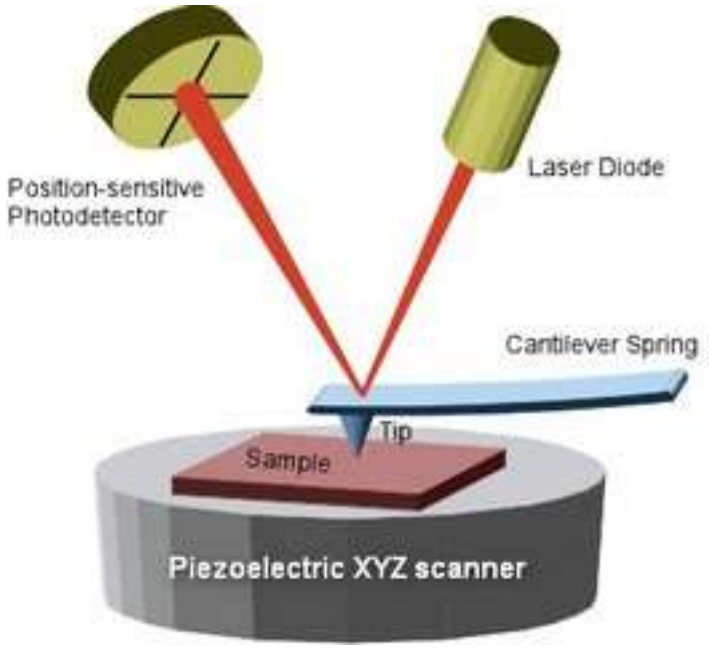

Figure 1: Atomic force microscopy illustration, (Fielden, 2017).

$$k_s = 2a\left(\frac{E_s}{1-{\nu_s}^2}\right) \qquad (2)$$

where k_s is the stiffness of the sample, a is the contact radius, and ν_s is the Poisson's ratio of the sample (Butt, Cappella, & Kappl, 2005). Alternatively, the elastic modulus can be calculated by fitting the force-displacement data to the Hertz model:

$$F = \frac{3E \cdot tan(\alpha)\delta^2}{4(1-\nu^2)} \qquad (3)$$

where F is the indentation force, E is the elastic modulus of the cell, α is the probing tip half angle, δ is the vertical displacement of the cantilever, and ν is the Poisson's ratio of the cell (MacKay J.L., 2012). AFM results are quite sensitive to vibration, temperature fluctuation, and interactions between the cell and the substrate surface; because of this uncertainty, elastic modulus values are sometimes reported as ratios rather than absolute values (Lekka, 2016). AFM requires the cell to be adhered to a substrate during testing, which changes the biomechanical

properties of the cell. A significant amount of preparation time is involved, reducing the ability of an AFM experiment to test for more transient biomechanical effects.

Optical tweezers employ a focused laser to trap dielectric microparticles such as individual molecules, silica beads, or single cells. The interaction between the photons and the particle changes the direction of the photon's path. This change in direction results in a momentum transfer to the particle, displacing it slightly. The particle moves toward the center of the laser beam, where the light intensity is greatest, to minimize its energy and balance the forces between the light and the particle (Dholakia & Reece, 2006; Neuman & Block, 2004). This is referred to as trapping; at its lowest energy state, the particle is held stationary in three dimensions. The forces holding the particle in the trap are generally on the order of piconewtons, and depend on the stiffness of the trap (related to the light intensity of the laser) and the size of the particle (H. Zhang & Liu, 2008). Biological cells are often too large to hold securely in an optical trap, and the photons from the laser can impart thermal damage to the cell (H. Zhang & Liu, 2008). For this reason, silica microbeads are often attached to the cell membrane and used as handles to manipulate the cell, avoiding direct irradiation of the cell with photons. A typical configuration includes a bead fixed to a stage, with a cell attached to the bead. Another bead is attached to the other side of the cell and trapped in the laser beam. Either the stage or the laser

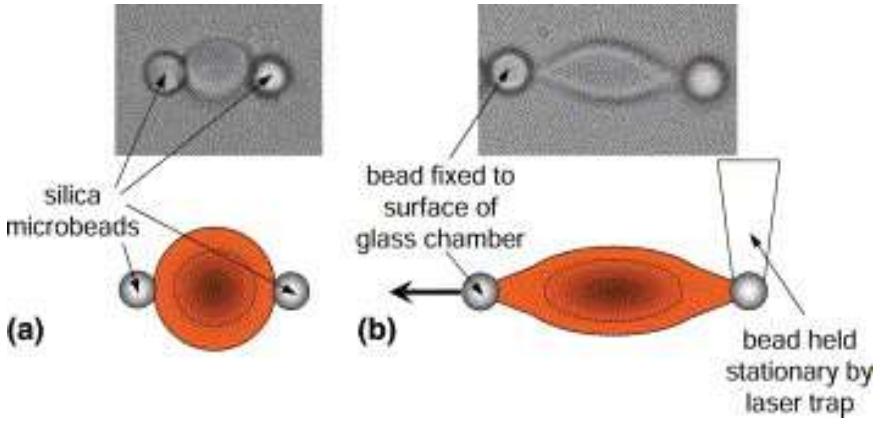

Figure 2: Optical tweezers. Silica beads are attached to a red blood cell; movement of one of the beads stretches the cell axially. Reproduced without permission from (Lim, Dao, Suresh, Sow, & Chew, 2004).

beam may be displaced, stretching the cell between them. This process is illustrated in Figure 2. The optical tweezer method can be used to quantify cell rotation speed, membrane shear stress, shear modulus, and viscoelasticity (Bronkhorst et al., 1995; Guck et al., 2005; Henon, Lenormand, Richert, & Gallet, 1999; Lim et al., 2004). However, the forces generated by this method are usually not strong enough to rupture the cell membrane; the beads detach from the membrane before it tears, making optical tweezers insufficient to study the failure strength of cell membranes.

Microfluidic deformability cytometry is used to study whole-cell deformability by passing cells in solution through microfluidic channels. An example of a microfluidic cytometry channel is shown in Figure 3. This method allows the calculation of the size and deformation of hundreds or thousands of cells per second, making it easily the highest throughput option for determining cell characteristics. Cells are modeled as elastic shells or elastic solids, and assumed

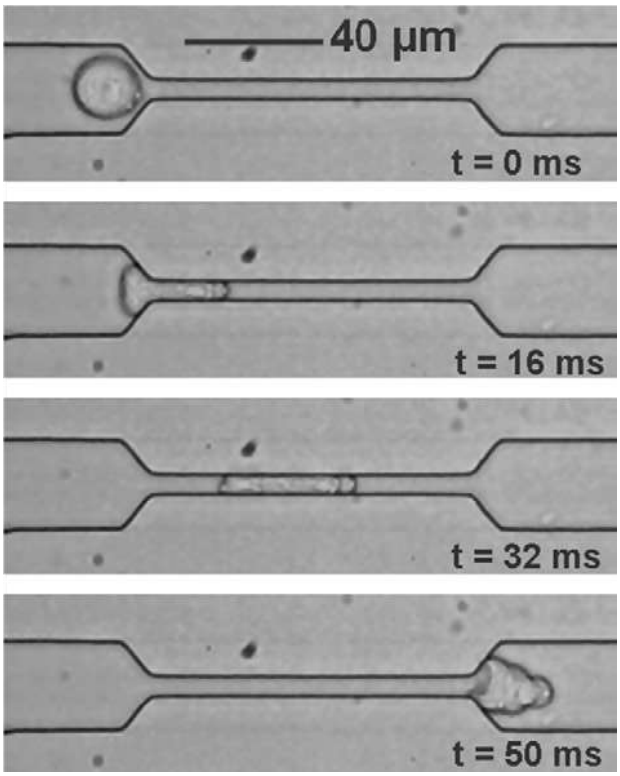

Figure 3: Microfluidic deformability cytometry.
Panc-1 cancer cell moves through PMDS channel.
Reproduced without permission from (Suresh, 2007).

to be homogeneous and incompressible. Simultaneous fluorescence measurements can also provide information about cell biochemical properties. The size of the channel relative to the diameter of the cell will influence the flow characteristics and the relevant measurements. For channels larger than the cell diameter, the fluid shear stress imposed on the cells causes a shape change related to the cell stiffness. The cell does not contact the channel walls or other cells, so the only forces acting on it are the pressure gradient and fluid shear stress (Gossett et al., 2012). For channels smaller than the cell diameter, measurements include the time required for the cell to completely enter the constriction, transit time through the channel, and elongation of the cell (Lange et al., 2015). These measures are used to calculate cell strain, stiffness, elastic modulus and viscosity (Gossett et al., 2012; Huang, Bow, Diez-Silva, & Han, 2011; Mietke et al., 2015).

Micropipette aspiration (MPA) is a single-cell manipulation technique developed by Mitchison and Swann (Mitchison & Swann, 1954). A small glass pipette filled with water, with a diameter roughly half the diameter of the cell, interacts with a cell in solution on a glass slide under a microscope. The pipette, controlled by a micromanipulator, is connected through a continuous series of tubing to a water column which can be raised and lowered to change the

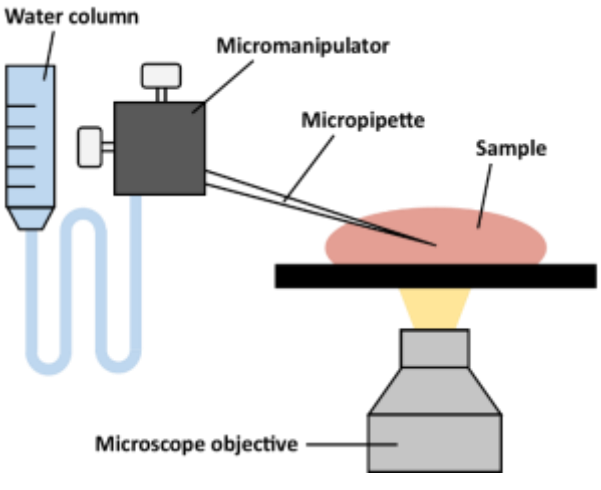

Figure 4: Micropipette aspiration illustration.

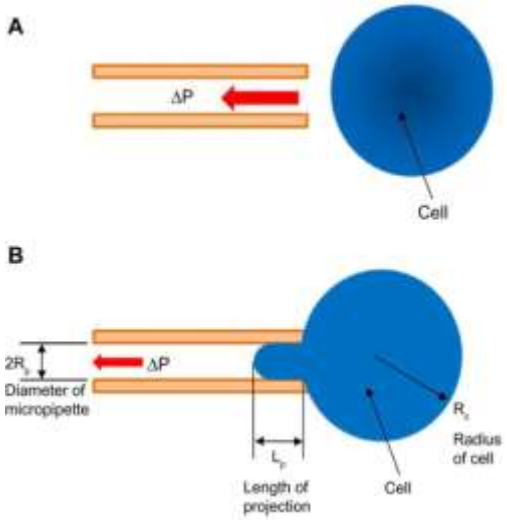

Figure 5: Parameters measured during micropipette aspiration. Reproduced without permission from (Chivukula, Krog, Nauseef, Henry, & Vigmostad, 2015)

hydrostatic pressure at the tip of the pipette. The system is illustrated in Figure 4. This method has been used to investigate cell-substrate adhesive forces (Hogan, Babataheri, Hwang, Barakat, & Husson, 2015); cell-cell adhesive forces (Biro & Maitre, 2015); and whole-cell elastic modulus (Hochmuth, Mohandas, & Blackshear Jr., 1973; Jones, 1999), cortical tension (Hochmuth, Ting-Beall, Beaty, Needham, & Tran-Son-Tay, 1993; Lam, Herant, Dembo, & Heinrich, 2009), viscosity (E. A. Evans, Yeung, A., 1989), and viscoelasticity (Chien, Sung, Skalak, Usami, & Tozeren, 1978). Commonly measured parameters of the MPA experiment include the length of the membrane projection inside the pipette, the diameter of the pipette, the total area of the cell, and the time of relaxation of the cell, illustrated in Figure 5. The assay does not require cell adherence to a surface, preparation time is minimal, and membrane rupture can be achieved and easily observed, making micropipette aspiration a suitable option for this analysis.

1.3 Cancer Cell Mechanical Properties

The methods discussed in the previous section have been used to characterize the mechanical properties of many types of cells under various conditions. Table 1 presents the findings of several studies using these methods to characterize cancer cells. To summarize their findings, it is commonly discovered that cancer cells have a lower baseline elastic modulus and cortical tension than non-cancerous cells. Methods used in the studies included atomic force microscopy, deformability cytometry, micropipette aspiration, and optical tweezers.

1.4 Objectives

The purpose of this study was to characterize the mechanical properties of cancer cells, to document how these properties change after exposure to a high level of fluid shear stress, and to develop a computational model to describe local stresses in the cell membrane. The variables studied were elastic modulus and rupture pressure during micropipette aspiration. The cell lines used were prostate epithelial cells (PrEC) and transformed prostate cancer cells (PC-3).

Table 1: Mechanical properties of cancer cells compared to non-cancerous cells.

Tissue	Cell Line	Experiment	Mechanical properties	Results	Reference
Bladder	Hu609, Hu456	Atomic force microscopy	Elastic modulus	E(Hu609) = 9.7 kPa, E(Hu456) = 0.3 kPa	(Lekka et al., 1999)
Bladder	HCV29, HTB-9	Atomic force microscopy	Elastic modulus	E(HCV29) = 10-50 kPa, E(HTB-9) = 5-15 kPa	(Ramos, Pabijan, Garcia, & Lekka, 2014)
Prostate	BPH, PC-3	Atomic force microscopy	Elastic modulus	E(BPH) = 2.80 kPa, E(PC-3) = 1.40 kPa	(Faria et al., 2008)
Prostate	PZHPV-7, PC-3, DU145	Atomic force microscopy	Elastic modulus	E(PZHPV) = 3.09 kPa, E(PC-3) = 1.95 kPa, E(DU145) = 1.36 kPa	(Lekka et al., 2012)
Prostate	Vero, DU145	Atomic force microscopy	Elastic modulus	E(Vero) = 1.3 kPa, E(DU145) = 0.60 kPa	(Efremov et al., 2015)
Bladder	RT4	Deformability cytometry	Cortical tension	CT(RT4) = 185 μN/m	(Guo, Park, & Ma, 2012)
Breast	MCF-7, MDA-MB-231	Deformability cytometry	Elastic modulus	E(MCF-7) = 2.1 kPa, E(MDA) = 0.80 kPa	(Nyberg et al., 2017)
Breast, Leukemia	MDA-MB-231, K296	Deformability cytometry	Elastic modulus	E(MDA) = 575 Pa, E(K296) = 296 Pa	(Lange et al., 2015)
Leukemia	HL60	Deformability cytometry	Elastic modulus	E(HL60) = 1.48 kPa	(Mietke et al., 2015)
Leukemia	Jurkat	Micropipette aspiration	Viscoelastic coefficients	K_1(Jurkat) = 83.2 N/m², μ(Jurkat) = 4.1 Pa·s	(Chen et al., 2004)
Liver	HTC, HCC (SMMC 7721)	Micropipette aspiration	Viscoelastic coefficients	K_1(HTC) = 87.5 N/m², K_1(HCC) = 103.6 N/m², μ(HTC) = 5.9 Pa·s, μ(HCC) = 4.5 Pa·s	(G. Zhang, Long, Wu, & Yu, 2002)
Prostate	PrEC LH, PC-3	Micropipette aspiration	Elastic modulus, cortical tension	E(PrEC) = 47.7 Pa, E(PC-3) = 20.0 Pa, CT(PrEC) = 346 μN/m, CT(PC-3) = 135 μN/m	(Chivukula et al., 2015)
Breast	MCF-7, MDA-MB-231	Optical stretching	Optical deformability	OD(MCF-7) = 21.4%, OD(MDA) = 33.7%	(Guck et al., 2005)
Breast	MCF-7, MDA-MB-231	Optical stretching	Elastic modulus	E(MCF-7) = 31.6 Pa, E(MDA) = 12.6 Pa	(Yousafzai, 2016)

CHAPTER 2: MATERIALS AND METHODS

2.1 Cell Culture

Experiments were performed using transformed prostate cancer cells (PC-3), obtained from the American Type Culture Collection, and immortalized, non-transformed prostate epithelial cells (PrEC), obtained from Dr. William Hahn (Dana-Farber Cancer Institute). PC-3 cells were cultured in DMEM/F12 medium with 10% fetal bovine serum, while PrEC cells were cultured in Lonza's PrEGM medium, according to recommended guidelines. Cells were released from plates using 0.25% trypsin and resuspended in medium to a concentration of about $5 \cdot 10^5$ cells/mL immediately prior to experimentation.

2.2 Micropipette Fabrication

Borosilicate glass pipettes (OD 1.0 mm, ID 0.75 mm) were obtained from World Precision Instruments. The pipettes were pulled to a fine, tapered end by using Sutter Instruments' P-30 Vertical Micropipette Puller (Figure 6). The operation of the pipette puller is simple: a pipette is held in place at the top end and fixed to a weight at the bottom end, with the center of the pipette passing through a Nichrome filament. When the puller is activated, the filament heats up, heating the glass pipette to a softening point. The soft glass stretches under the force of gravity until it triggers a switch that turns off the heat and pulls the pipette down, creating a clean break between the two halves of the pipette ("P-30 Micropipette Puller Operation Manual," 2013). The pipettes pulled in this manner had very narrow tips, so further processing was needed. The glass pipettes were cut to the correct tip diameter using a Narishige MF-900 Microforge (Figure 7). A glass bead surrounds a heating filament; the entire assembly can be adjusted in three dimensions. The pipette is positioned next to the glass bead; when the filament is activated, the heat causes the glass pipette to briefly fuse with the bead. The heat is then released, and the pipette is pulled sharply away from the bead. If performed correctly, the end of the pipette is cut cleanly at the desired diameter. A ruler is set into the eyepiece to measure the

Figure 6: Sutter Instruments pipette puller, ("P-30 Vertical Micropipette Puller," 2012).

Figure 7: Narishige microforge, ("MF-900 Microforge," 2018).

width of the pipette tip. Pipettes were cut to approximately 7-8 μm inner diameter and stored in a closed container to reduce risk of contamination or fracture.

2.3 Fluid Shear Stress Assay

Cells were exposed to fluid shear stress by infusing the cells in solution through a small-bore needle, replicating the method used by Chivukula (Chivukula et al., 2015). After the cells were deplated, they were diluted to approximately $5 \cdot 10^5$ cells/mL. An infusion pump (Harvard Apparatus, PHD 2000 Infusion/Withdraw Pump, Figure 8) was set to infuse 250 μL/s through a 30-gauge needle, exposing the cells to fluid shear stress. The cells were subjected to ten passages through the needle immediately before the micropipette aspiration experiment. The maximum shear stress experienced by the cells can be estimated by the Poiseuille equation, which assumes axisymmetric, laminar flow and a Newtonian fluid:

$$\tau = \frac{4Q\mu}{\pi R^3} \qquad (4)$$

Figure 8: Harvard Apparatus syringe pump,
("Standard Infuse/Withdraw PHD ULTRA™
Syringe Pumps," 2018)

where τ is the wall shear stress, Q is the flow rate, μ is the dynamic viscosity of the medium (0.01 dyn·s/cm^2), and R is the radius of the needle. Characterization of flow as laminar or turbulent is determined by the Reynold's number, which can be calculated by the following equation,

$$Re = \frac{4Q\rho}{\pi D\mu} \cong 210 \qquad (5)$$

where ρ is the density of the fluid (1.0 g/mL) and D is the inner diameter of the needle (0.16 mm). Even using conservative estimates of dynamic viscosity and density for the culture medium, the Reynold's number is well under the critical value of 2000, which supports the use of Poiseuille flow to describe the shear stress experienced by the cells in the assay. The maximum shear stress, calculated to be 6200 dyne/cm^2, is experienced by cells near the wall of the needle. Shear stress decreases linearly with distance from the wall, with the cells traveling near the centerline experiencing the minimum shear stress.

$$\tau = \frac{\tau_w r}{R} \qquad (6)$$

In this equation, τ is the shear stress at location r, which is the radial distance from the centerline; τ_w is the maximum shear stress at the wall; and R is the total radius of the channel. To calculate

the minimum shear stress experienced by cells traveling at the centerline of the needle, the radius of the cell is substituted for *r* (average 10 μm). This results in a minimum shear stress of 775 dyne/cm^2.

2.4 Micropipette Aspiration

To determine the cells' mechanical properties, micropipette aspiration was performed on PC-3 and PrEC cells. A micropipette was filled with PBS and connected to a series of Tygon tubing filled with distilled water, which was connected to the water column. Care was taken to avoid air bubbles in any part of the pipette or tubing, as these would interfere with the hydrostatic pressure applied by the water column. The pipette was calibrated to a zero pressure point by adding or removing water from the column. Positive or negative pressure could be clearly observed by placing a few drops of a solution containing polyethylene beads under the Nikon Diaphot 300 microscope (Figure 9); the beads flowed away from or toward the open end of the pipette under positive or negative pressure, respectively. Water was added to or removed from the water column until there was no motion observed from the beads near the tip of the pipette. After

Figure 9: Nikon Diaphot 300 microscope, ("Nikon DIAPHOT-300 Research-Grade Biotech Inverted Microscope," 2015).

Figure 10: Scientifica LBM-7 micromanipulator, ("LBM-7 Manual Manipulator," 2015).

cells were deplated, they were diluted in medium, and a few drops of the solution were placed on a glass slide under the microscope. Using a Scientifica LBM-7 micromanipulator (Figure 10), the pipette was positioned almost horizontally near a target cell. Individual target cells were chosen based on size and appearance; the size of the cell should be at least twice the diameter of the pipette, and the cell's texture should appear healthy and normal. The pressure was reduced in the pipette by lowering the water column by 5 mm in order to suck the cell against the pipette opening, forming a seal. The cell was then lifted off the surface of the slide. The cell was allowed to equilibrate to the applied negative pressure. An image was then captured using Allied Vision's Stingray F080C microscope camera (Figure 11) and SmartView software, and the pressure was lowered again by another 5-mm increment. This continued until the cell membrane ruptured or the maximum lowering distance of the water column was reached (50 mm). The pressure was then raised to zero, and the cell was allowed to detach from the pipette. Recalibration of the water column was sometimes required to reset the zero pressure point before picking up a new cell.

In some cases, the suction pressure in the pipette was increased past 50 mmH_2O by removing water from the water column. The inner diameter of the syringe containing the water column was reported as 26.7 mm (Harvardapparatus.com); the volume of water to be removed from the water column was therefore calculated to be 2.8 mL for a 5-mm decrease in height. A syringe was used to remove water from the column to decrease the pressure further past 50 mmH_2O. The upper limit of this method was 100 mmH_2O negative pressure. The precision of this method is admittedly lower than using the micrometer; the volume of water removed by the syringe can be measured to within 0.2 mL, corresponding to a height difference of about 0.4 mm.

Figure 11: Allied Vision Stingray microscope camera, ("Stingray F-080,").

The micrometer is accurate to 0.01 mm. However, this method proved useful to determine how close the cells were to rupturing at 50 mmH_2O, as well as confirming the continued linear relationship between applied pressure and projection length at higher pressure levels.

2.5 ImageJ Analysis

ImageJ software was used for post-processing the images gathered during MPA. The tool allows the user to measure distances and coordinates of plotted points. This was the method used to determine the diameter of the cell, the diameter of the pipette, the projection length of the cell, the height of the projection cap, and the points plotted along the membrane cap.

2.6 Elastic Modulus

The whole-cell elastic modulus was calculated using the model developed by Theret et al., which assumes that the cell is a homogeneous elastic material (Theret, Levesque, Sato, Nerem, & Wheeler, 1988). Continuum models for biological materials are generally acceptable when the length scale of interest is significantly larger than the dimensions of the cytoskeletal elements (Mofrad & Kamm, 2006). For whole cell manipulation such as micropipette aspiration or microfluidic deformation, continuum models are appropriate. Theret evaluated two membrane displacement models for cells undergoing micropipette aspiration, the punch model and the force model, which differ in their boundary conditions. It was assumed that there was no friction between the cell and the pipette walls and that the deformation of the cell membrane was linear. The study concluded that the punch model more accurately describes the displacement of the cell membrane under an applied stress. The equation for elastic modulus was derived as:

$$E = \frac{3\Delta P R_p}{2\pi L_p}\Phi \qquad (7)$$

where ΔP is the difference in pressure across the cell, R_p is the radius of the pipette, L_p is the length of the projection aspirated into the pipette, and Φ is the wall function. The wall function is

a function of the wall parameter—the ratio of the pipette wall thickness to the pipette inner radius—and was solved for both the punch model and the force model. The punch model has a relatively consistent wall function over a range of wall parameters, reported as 2.1, which is commonly used to calculate elastic modulus (Chivukula et al., 2015; Hochmuth, 2000; Jones, 1999).

2.7 Projection Cap Shape

It has been postulated in a previous study that differences in rupture pressure between cancer and epithelial cells is due to the change in shape of the cell projection as it is drawn into the pipette (Wu, 2017). The shape of the projection cap (the rounded tip of the aspirated cell projection) does affect the stress distribution along the membrane; a rounder, regularly-shaped projection cap will have more evenly distributed stress than an irregular or flattened cap. Stress concentrations are likely to contribute to the rupture pressure and location of rupture along the membrane. This cap shape hypothesis was investigated in this study by using ImageJ to measure the height of the projection cap inside the pipette. Height was defined as the vertical distance between the apex of the projection and the intersection of the membrane with the pipette wall. This distance was normalized by the pipette radius. Normalized cap height values close to 1.0 should represent cells with rounder, more spherical projection caps. Cap heights were measured at multiple pressure levels for a subset of cells in each experimental group undergoing micropipette aspiration.

2.8 Membrane Stress Analysis: MATLAB

During micropipette aspiration, a pressure difference is created across the cell, causing a portion of the membrane to be aspirated into the pipette. The cell membrane stretches and distorts as it is pulled into the narrow pipette, creating stress in the membrane. The mechanical stress in the projection cap can be solved for by computationally modeling the curvature of the membrane

at a known applied pressure. A MATLAB model, first developed by Wu, was modified and extended for use in this analysis (Wu, 2017).

The stress model used in this analysis has several assumptions to be declared. The cell membrane is assumed to have a negligible bending modulus and constant cortical tension. The projection cap is also assumed to be axisymmetric. Boundary conditions were applied at both ends of the curve: the curve is horizontal at the apex and vertical where it meets the pipette wall.

ImageJ software was used to place points marking the edge of the cell membrane using the images recorded at different aspiration pressures during MPA. An example of this procedure is shown in Figure 12. The x-y cartesian coordinates of these points were imported into MATLAB and normalized to place the apex at x=0 and the pipette wall at x=1. A 2-piece, 3rd-order polynomial spline was fitted to the points, using the "splinefit" function authored by Lundgren (Lundgren, 2011). The spline is described by two parametric equations that are functions of the arclength, *s*, of the curve.

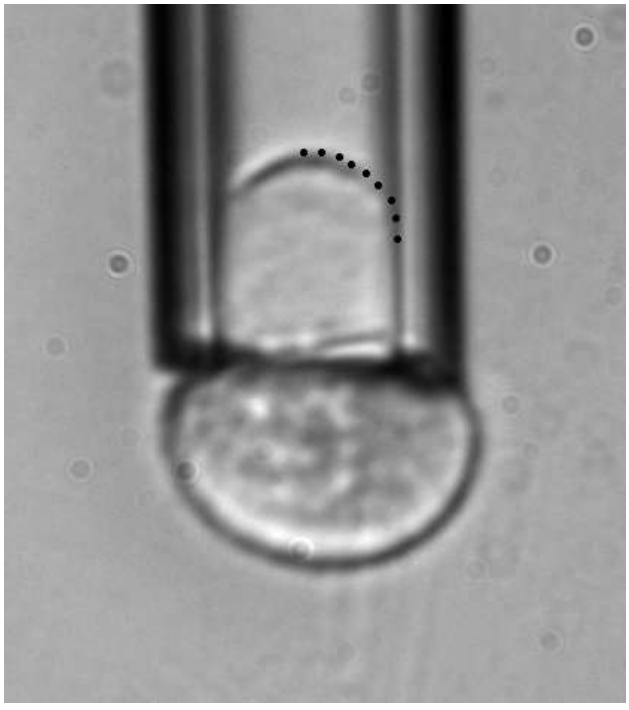

Figure 12: Points plotted along membrane curve in ImageJ.

$$x_i(s) = C_{X1}(s_i - b)^3 + C_{X2}(s_i - b)^2 + C_{X3}(s_i - b) + C_{X4} \quad (8)$$

$$y_i(s) = C_{Y1}(s_i - b)^3 + C_{Y2}(s_i - b)^2 + C_{Y3}(s_i - b) + C_{Y4} \quad (9)$$

In these equations, *C* refers to the polynomial coefficients of the spline, *s* is the arclength, and *b* is the location of the closest previous break point. The break point marks the boundary between each piece in the spline. The derivatives of these functions, with respect to arclength, were calculated using both MATLAB's "diff" function, which calculates the true derivative of the polynomial equation, and the central difference method, which calculates the local derivative based on surrounding points on the curve. The central difference method is defined as:

$$\left(\frac{dx}{ds}\right)_i = \frac{x_{i+1} - x_{i-1}}{s_{i+1} - s_{i-1}} \quad (10)$$

$$\left(\frac{dy}{ds}\right)_i = \frac{y_{i+1} - y_{i-1}}{s_{i+1} - s_{i-1}} \quad (11)$$

$$\left(\frac{d^2x}{ds^2}\right)_i = \frac{x_{i+1} - 2x_i + x_{i-1}}{\Delta s^2} \quad (12)$$

$$\left(\frac{d^2y}{ds^2}\right)_i = \frac{y_{i+1} - 2y_i + y_{i-1}}{\Delta s^2} \quad (13)$$

where *Δs* is the average arclength distance between adjacent points. It was found that there was a negligible difference between the two methods used to calculate the derivatives, so the "diff" function was chosen based on speed of computation.

The local meridional and circumferential curvatures were then calculated from the x- and y-derivatives with respect to arclength. The equations to define these curvatures are:

$$k_M = \frac{x'y'' - y'x''}{(x'^2 + y'^2)^{1.5}} \quad (14)$$

$$k_C = \frac{\sin\left(arctan\left(\left|\frac{y'}{x'}\right|\right)\right)}{r} \quad (15)$$

where k_M is the meridional curvature, k_C is the circumferential curvature, and r is the horizontal distance to the centerline of the axisymmetric curve. The prime notations x' and x'' refer to the first and second derivatives with respect to arclength, respectively. The two curvatures must be equal at the apex of the curve. The curvatures were then used to calculate principal stresses T_1 and T_2:

$$T_1 = \frac{\Delta P}{2k_C} \qquad (16)$$

$$T_2 = \Delta P\left(\frac{2k_C - k_M}{2{k_C}^2}\right) \qquad (17)$$

where ΔP is the applied negative pressure from the pipette (E. A. Evans, 1973). These stresses are illustrated in Figure 13. The pressure is calculated by the hydrostatic pressure equation:

$$\Delta P = \rho g \Delta h \qquad (18)$$

Where ρ is the density of the fluid (1.0 g/mL), g is the acceleration of gravity, and Δh is the difference in height between the surface of the water column and the microscope stage.

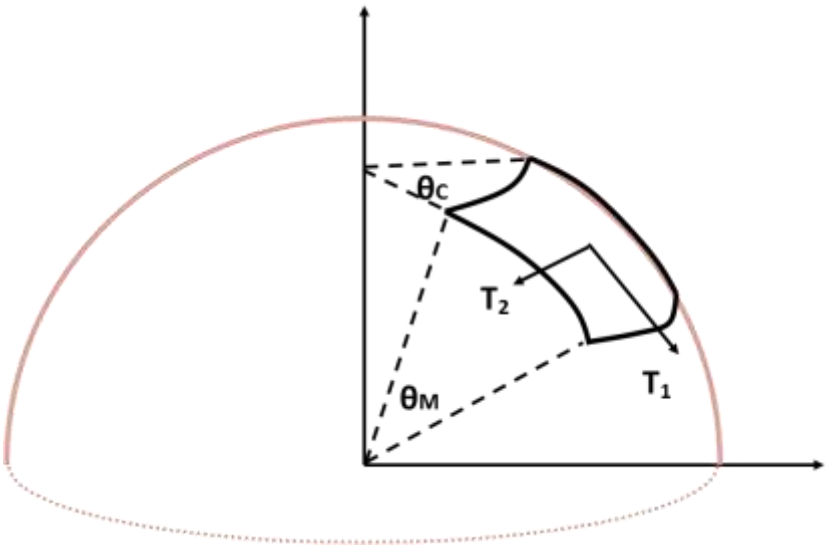

Figure 13: Principal stresses of hemispherical membrane. T_1 is the principal stress in the meridional direction. T_2 is the principal stress in the circumferential direction.

The principal stresses can be used to calculate von Mises stress by the following equation:

$$von\ Mises = \sqrt{{T_1}^2 - T_1T_2 + {T_2}^2} \qquad (19)$$

The use of von Mises stress requires the assumption that the material is incompressible, which is a generally accepted assumption for biological materials. This study will focus on the development of principal stresses and von Mises stress in the cell membrane.

2.9 Membrane Stress Validation: Abaqus

To validate the results of the MATLAB model of the max/min locations and relative amplitudes of the membrane stress, a finite element model was constructed using Abaqus 6.14 software to represent the cell membrane during micropipette aspiration. Axisymmetric, linear membrane elements were used to represent the spline fitted to the data by MATLAB. The thickness of the membrane was assigned to be 1 unit (total horizontal length of the curve was 100 units), and the Poisson's ratio was set to 0.49. The membrane was modeled as a Neo-Hookean, isotropic, hyper-elastic material. The bulk and shear moduli were set to arbitrarily high values to limit deformation of the membrane ($1.0 \cdot 10^6$ units and $1.0 \cdot 10^4$ units, respectively), because the fitted spline represents the already deformed membrane during MPA. The non-linear geometry option was activated, and boundary conditions were implemented at the end nodes to restrict displacement. The apex node was constrained in the x-direction, and the base node at the wall was constrained in the x- and y-directions. A small body force load was applied to the cap portion of the membrane in the positive y-direction to simulate the negative pressure applied to the membrane during MPA. Figure 14 illustrates the Abaqus model with loading and boundary conditions.

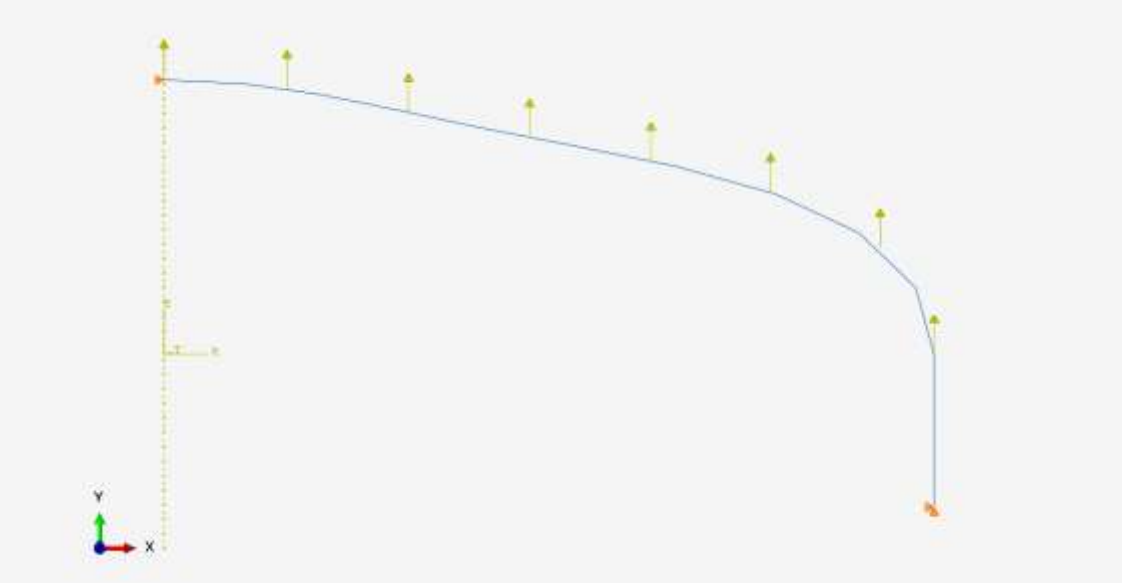

Figure 14: Abaqus model of projection cap of PC-3 cell during micropipette aspiration. Model employed axisymmetric membrane elements with applied body force (yellow arrows) to simulate negative pressure during aspiration. Orange arrows at the endpoints represent displacement boundary conditions.

CHAPTER 3: RESULTS

3.1 Micropipette Aspiration

Data were gathered for rupture pressure, elastic modulus, and dimensions of cells undergoing micropipette aspiration. The delay time was also recorded for each cell. For unsheared cells, delay time was defined as the time elapsed between removing the cells from the culture dish and lifting an individual cell off the microscope slide to begin the MPA experiment; for sheared cells, delay time was defined as the time elapsed between the end of the fluid shear stress assay and lifting the cell off the microscope slide for MPA. The total numbers of cells used for the micropipette aspiration experiments in each group are presented in Table 2. Example images of a PC-3 cell during MPA are presented in Figure 15.

Table 2: Numbers of cells used in each experimental group.

	PC-3	**PrEC**
Unsheared	62	16
Sheared	30	15

3.1.1 Confounding Variables

It is a general rule to only use cells in a micropipette experiment within an hour after they are removed from the culture dish. For this reason, the elastic modulus and rupture pressure were evaluated for differences between measurements taken within 60 minutes of delay time and outside 60 minutes of delay time. Significant differences were found for rupture pressure between the time categories (unpaired t-test, all experimental groups pooled, p-value = 0.0072), but not for elastic modulus (Figure 16 and Figure 17). When the data were further split into groups by exposure to shear stress, there was still no difference in elastic modulus between sheared and unsheared cells in the different time groups (Figure 18), but it was observed that the change in rupture pressure with time is only evident in the cells exposed to shear stress (Figure 19). There was no change with time for the cells that were not exposed to shear stress. Of the cells that were exposed to shear stress, the rupture pressure was significantly higher for the cells measured

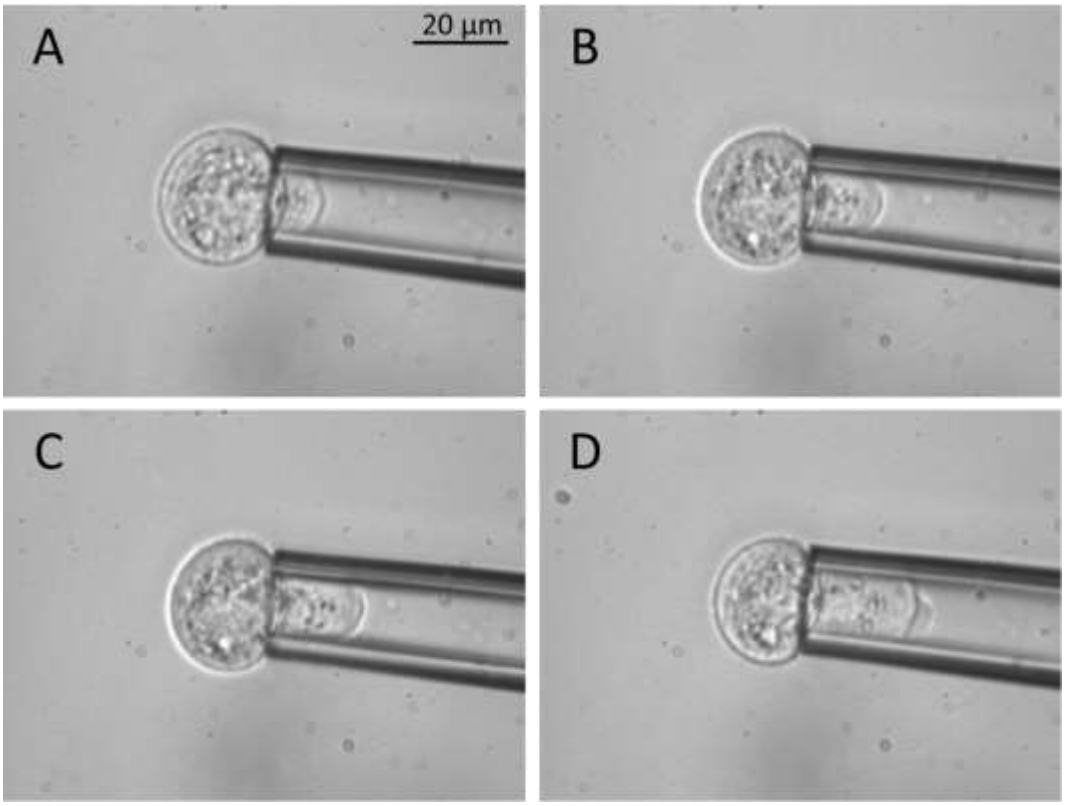

Figure 15: Micropipette aspiration example images, unsheared PC-3. A: 10 mmH_2O, B: 15 mmH_2O, C: 20 mmH_2O, D: Cell membrane ruptured at 25 mmH_2O.

within 60 minutes of delay time. This difference was detected by a one-way ANOVA with the Tukey test to correct for multiple comparisons. The shear stress group tested within 60 minutes delay time had a significantly higher rupture pressure from every other group. When the sheared cells were further grouped by cell type, it was observed that the PrEC cells continued the pattern of decreased rupture pressure with time. There were too few sheared PC-3 cells measured after 60 minutes delay time to make a similar comparison for that experimental group. This data is presented in the Appendix, Figure A.1. It was decided to limit the experimental findings to data gathered within 60 minutes delay time, to remove time as a confounding variable.

Other confounding variables were tested, including cell diameter and ratio of cell diameter to pipette size (D_c/D_p). All experimental groups were pooled together to test for a correlation between cell diameter or D_c/D_p versus rupture pressure or elastic modulus. The results

are presented in Table 3. Two significant correlations were found among the comparisons of the pooled data. Cell diameter was negatively correlated with rupture pressure, indicating that larger cells tended to rupture at lower pressures, and D_c/D_p was negatively correlated with elastic modulus, indicating that the measured elastic modulus was higher for cells that were smaller in relation to the pipette size. When the data were split by cell type and analyzed again, cell diameter and D_c/D_p were found to be negatively correlated with elastic modulus for PrEC cells,

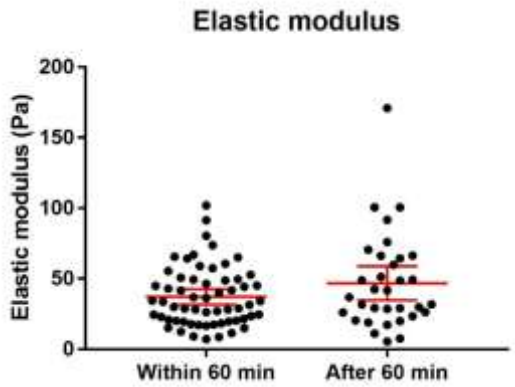

Figure 16: Elastic modulus measured within 60 minutes delay time and after 60 minutes delay time. Comparison was not significant (p = 0.0946). Error bars represent 95% confidence interval for the mean.

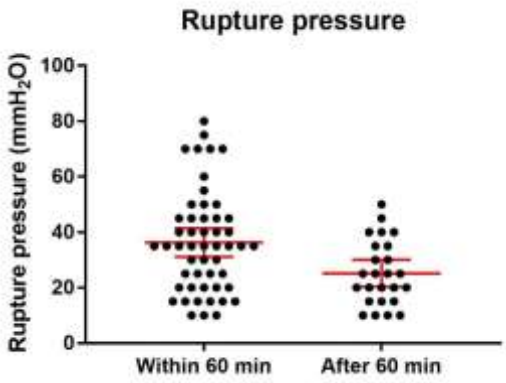

Figure 17: Rupture pressure measured within 60 minutes delay time and after 60 minutes delay time. Comparison was significant (p = 0.0072). Error bars represent 95% confidence interval for the mean.

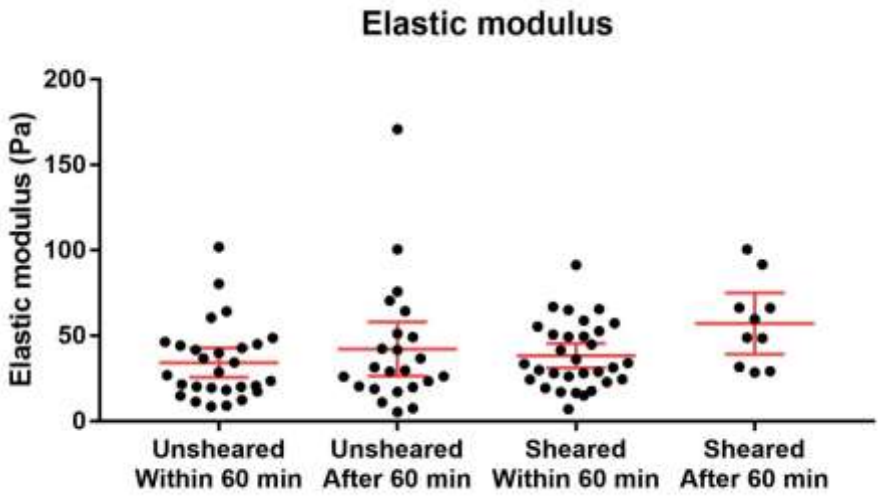

Figure 18: Elastic modulus measured within 60 minutes delay time and after 60 minutes delay time, grouped by exposure to shear stress. No significant differences between groups. Error bars represent 95% confidence interval for the mean.

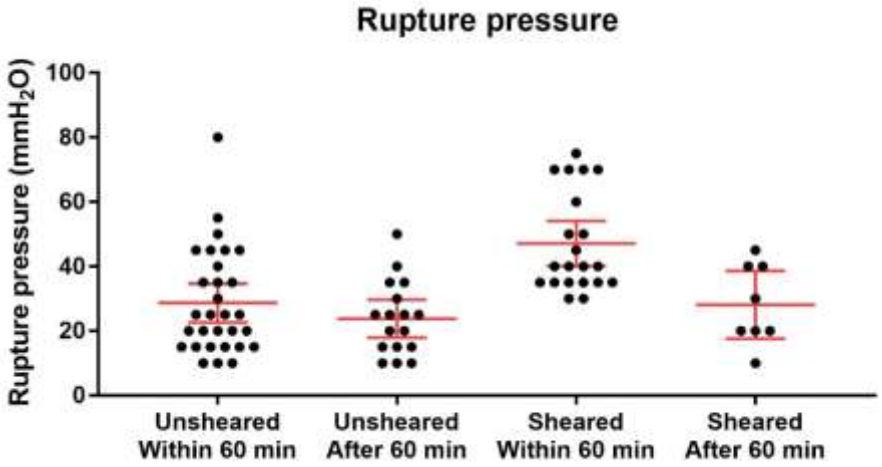

Figure 19: Rupture pressure measured within 60 minutes delay time and after 60 minutes delay time, grouped by exposure to shear stress. Significant differences between group exposed to shear stress and measured within 60 minutes and each other experimental group. Error bars represent 95% confidence interval for the mean.

indicating that larger PrEC cells tended to be less stiff. These correlation results are shown in Table 4. Physical explanations for this cell behavior are not immediately apparent. Other results and analyses were not restricted in any way to account or correct for these correlations between the cells' physical dimensions and material properties.

Table 3: Correlation results for pooled cell data. NS: Not Significant. R value indicates direction of correlation.

	Rupture Pressure	**Elastic Modulus**
Cell Diameter	R=-0.2521, p=0.0280	NS, p=0.1699
D_c/D_p	NS, p=0.0847	R=-0.2173, p=0.0344

Table 4: Correlation results for data grouped by cell type. NS: Not Significant. R value indicates direction of correlation.

	Rupture Pressure		**Elastic Modulus**	
	PC-3	**PrEC**	**PC-3**	**PrEC**
Cell Diameter	NS, p=0.1282	NS, p=0.2139	NS, p=0.8848	R=-0.6056, p=0.0028
D_c/D_p	NS, p=0.0802	NS, p=0.2065	NS, p=0.2320	R=-0.5194, p=0.0132

3.1.2 Elastic Modulus

An example of the calculation of elastic modulus for a PC-3 cell and a PrEC cell is presented in Figure 20. The length of the projection and diameter of the pipette were measured at several pressure points for a single cell; the pressure level was then plotted versus the ratio of projection length to pipette radius (L_p/R_p). Linear regression was applied to fit a line to the data; the slope of this line was used to calculate elastic modulus, using the Theret model described by Equation 7. This relationship between pressure and normalized projection length is remarkably linear; R-squared values were commonly between 0.95 and 0.99. Two values of elastic modulus were found to be statistical outliers by Grubb's test. Each value was an outlier in its individual experimental group (sheared PC-3's and unsheared PrEC's), and both were therefore excluded from the analysis. Average elastic modulus (values for each group are presented in the Appendix, Table A.1) was compared between groups using a one-way ANOVA with Tukey's test to correct for multiple comparisons. The results of this comparison, representing only cells measured within 60 minutes of delay time, are presented in Figure 21. There were significant differences for the means of elastic modulus between PC-3 unsheared versus PrEC sheared ($p = 0.0161$) and PC-3 sheared versus PrEC sheared ($p = 0.0172$). A histogram of elastic modulus for all groups at all

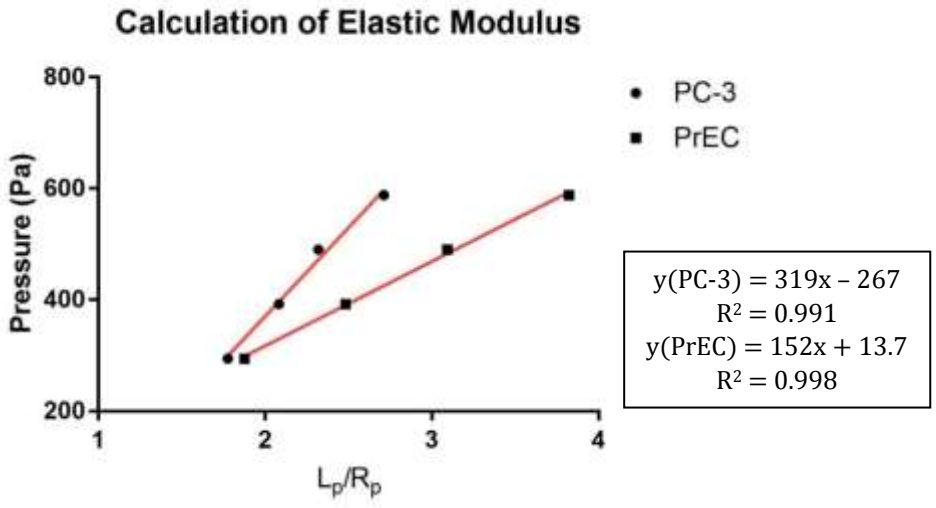

Figure 20: Example of calculation of elastic modulus. Linear regression is used to calculate the slope of the best fit line. Slope is then used to calculate elastic modulus.

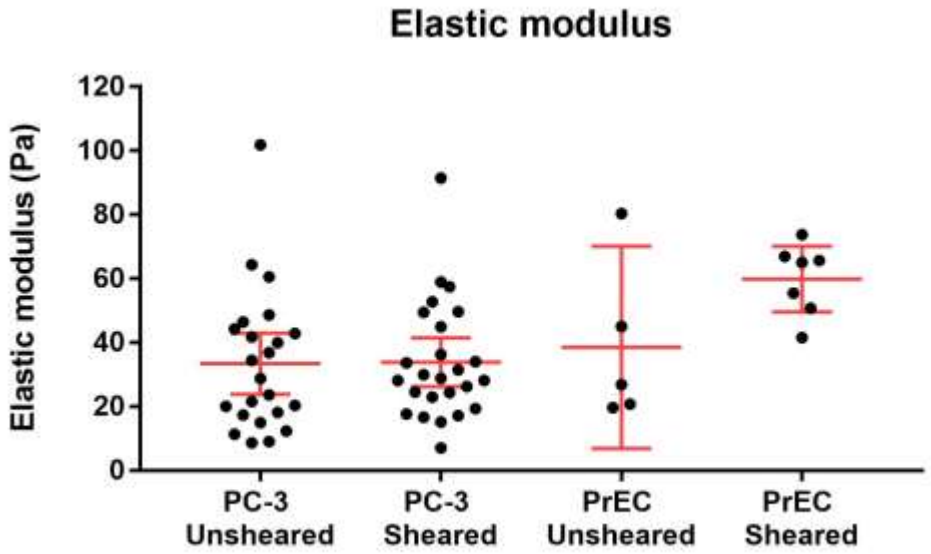

Figure 21: Elastic modulus assessed by micropipette aspiration. Significant differences between PrEC sheared group and both PC-3 experimental groups. Error bars represent 95% confidence interval for the mean.

time points is presented in Figure 22. The elastic modulus of cells that ruptured within 15 mmH_2O was sometimes impossible to calculate; the cell projection typically had not extended far enough into the pipette for the length to be reliably measured. This restricted the size of the experimental groups to a subset of the total number of cells used for MPA.

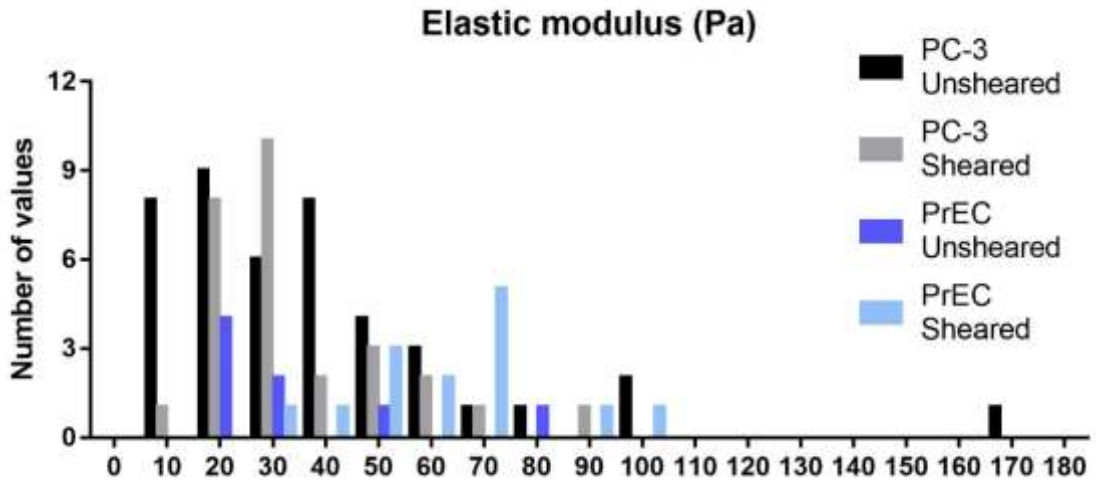

Figure 22: Histogram of elastic modulus for all experimental groups at all time points.

3.1.3 Rupture Pressure

Rupture pressure was recorded for each cell group during micropipette aspiration. A histogram of rupture pressure for each group is presented in Figure 23. As stated previously, only a portion of the cells ruptured within the maximum aspiration pressure applied during MPA. For earlier experiments, the max pressure was 50 mmH_2O, while for later experiments, 100 mmH_2O was reached. This makes the results somewhat difficult to interpret. Survival curves for each cell group (not accounting for delay time of the experiment) are presented in Figure 24. These curves were compared using the Log-rank test and the Gehan-Breslow-Wilcoxon test with Bonferroni's correction for multiple comparisons. These statistical tests account for censored subjects, or cells that did not reach a rupture point during the experiment. A significant difference was found between the survival curves for PC-3 unsheared vs PC-3 sheared cells ($p = 0.0050$). Median survival pressures (pressure at which 50% of the cells have ruptured) are presented in the Appendix, Table A.*2*.

The relative risk of rupture within 50 mmH_2O was also calculated for each group. The percentage of cells in each group that ruptured within 50 mmH_2O is presented in a graphical format in Figure 25. There were no significant comparisons in relative risk of rupture, though the

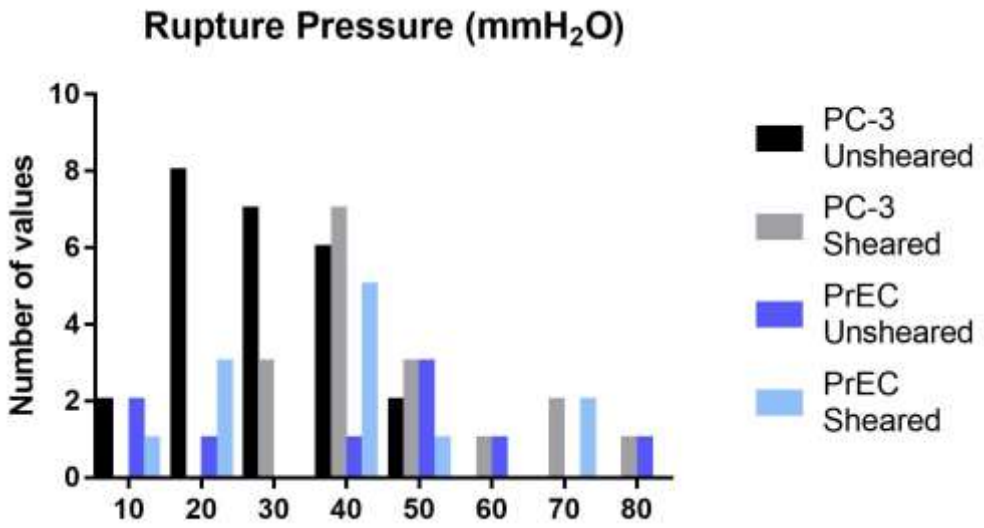

Figure 23: Histogram of rupture pressure for all experimental groups at all time points.

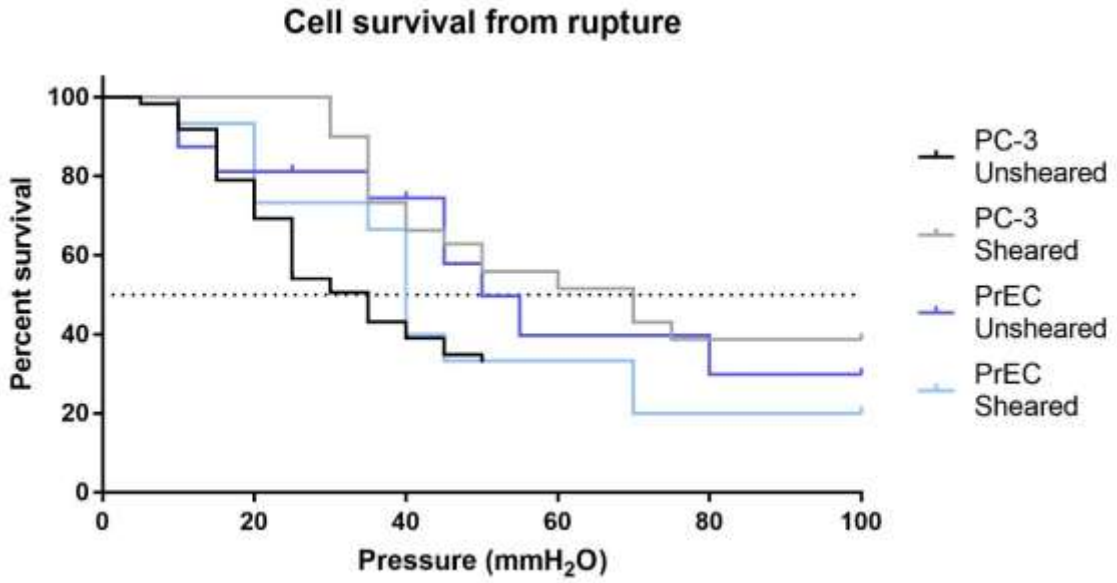

Figure 24: Rupture pressure survival curves. Significant difference between PC-3 unsheared and PC-3 sheared curves.

comparison between unsheared and sheared PC-3 cells was trending toward significance, with a relative risk of 0.68 and a p-value of 0.0962. This indicates that sheared PC-3 cells have 0.68 times the risk of rupturing within 50 mmH_2O as sheared PC-3 cells; in other words, the sheared cells survive higher pressures on average, though this difference was not found to be significant.

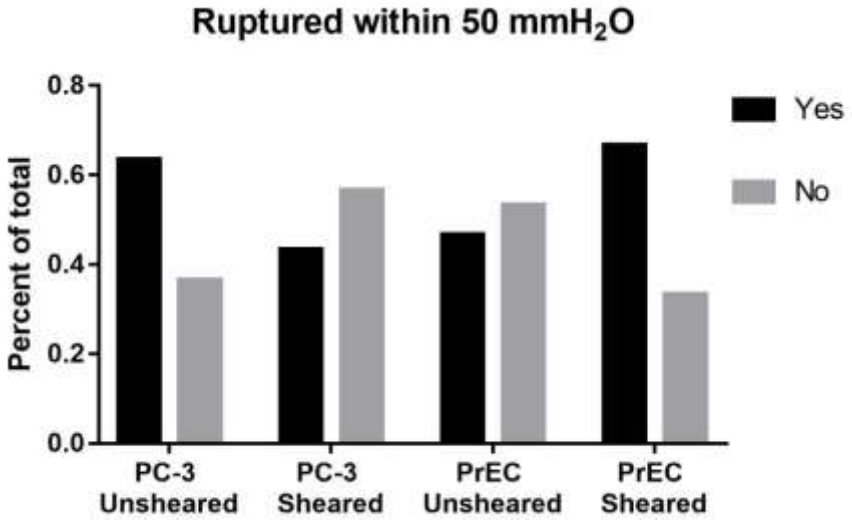

Figure 25: Percentage of cells within each experimental group that ruptured within an aspiration pressure of 50 mmH_2O.

It is worth noting that the unsheared PC-3 group resembles the sheared PrEC group, and that the sheared PC-3 group resembles the unsheared PrEC group in their rupture behavior. This is somewhat corroborated by the rupture survival curves in Figure 24; there is better overlap between the sheared PC-3 and unsheared PrEC curves, and between the unsheared PC-3 and sheared PrEC curves. However, especially for the PrEC groups, the low numbers of cells used in the experiments limit the ability of the tests to detect significant differences. Average rupture pressure between experimental groups was also analyzed using a one-way ANOVA with Tukey's test to correct for multiple comparisons, presented in Figure 26 (representing cells measured within 60 minutes delay time). It must be remembered, however, that these data represent only the cells that successfully ruptured during micropipette aspiration, and do not represent the cells that were not brought to a failure point. There were significant comparisons between several groups: PC-3 unsheared versus PC-3 sheared ($p = 0.0004$), PC-3 unsheared versus PrEC unsheared ($p = 0.0305$), and PC-3 unsheared versus PrEC sheared ($p = 0.0027$). Average values for rupture pressure are presented in the Appendix, Table A.2.

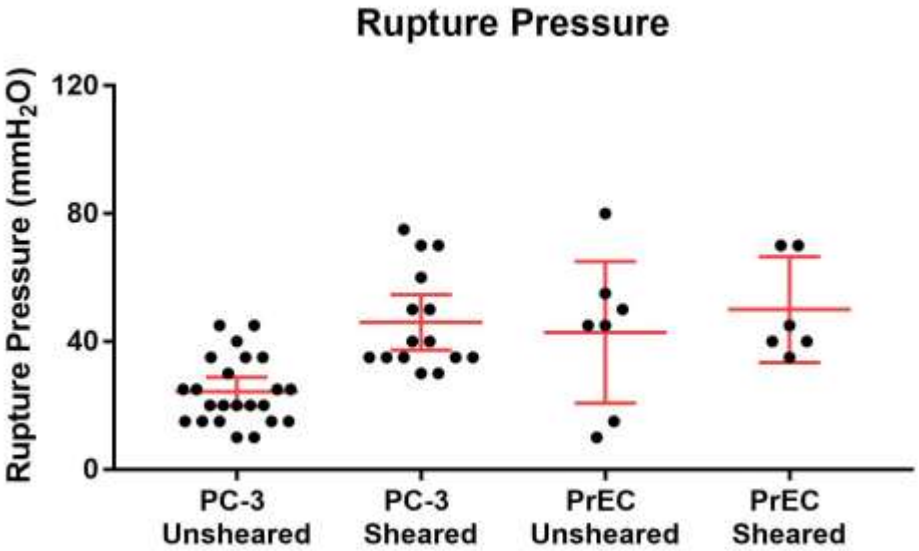

Figure 26: Rupture pressure between experimental groups. Significant differences between PC-3 unsheared versus PC-3 sheared, PC-3 unsheared versus PrEC unsheared, and PC-3 unsheared versus PrEC sheared groups. Error bars represent 95% confidence interval for the mean.

It was also investigated whether rupture pressure was related to elastic modulus. There was no correlation between rupture pressure and elastic modulus ($p = 0.4385$). Elastic modulus values were then split into groups based on whether the cell had ruptured within 50 mmH_2O. Using an unpaired t-test, no significant difference was found between groups ($p = 0.0659$). When elastic modulus values were categorized by cell type, exposure to shear stress, and successful rupture within 50 mmH_2O, two significant comparisons were found (One-way ANOVA with Tukey comparison). Sheared PrEC cells that did not rupture with 50 mmH_2O had a significantly higher elastic modulus than both sheared and unsheared PC-3 cells that did successfully rupture within 50 mmH_2O. Graphs of these results are presented in the Appendix, Figure A.2 and Figure A.3.

3.1.4 Projection Cap Shape

The height of the projection cap between groups was measured using ImageJ and analyzed. Cap heights were averaged between multiple pressure levels of individual cells and categorized by experimental group. The cap height at the pressure level just before rupture was also analyzed between experimental groups. No differences were found in either of these analyses (One-way ANOVA with Tukey comparison). Figures of these comparisons are presented in the Appendix, Figure A.4 and Figure A.5. A correlation analysis was also done for each group, to determine if the height of the projection cap significantly changes as pressure increases. These results are presented in Figure 27, along with linear regression lines to indicate the direction and magnitude of the correlation. Each marker in this figure represents the projection cap height of an individual cell at that pressure level; multiple data points were collected from each cell. There was a significant positive correlation between cap height and pressure for both of the sheared cell groups (PC-3, $p = 0.0306$; PrEC, $p = 0.0421$), indicating that the projection cap becomes taller or more rounded at higher pressures. However, the slope of the linear regression lines, while

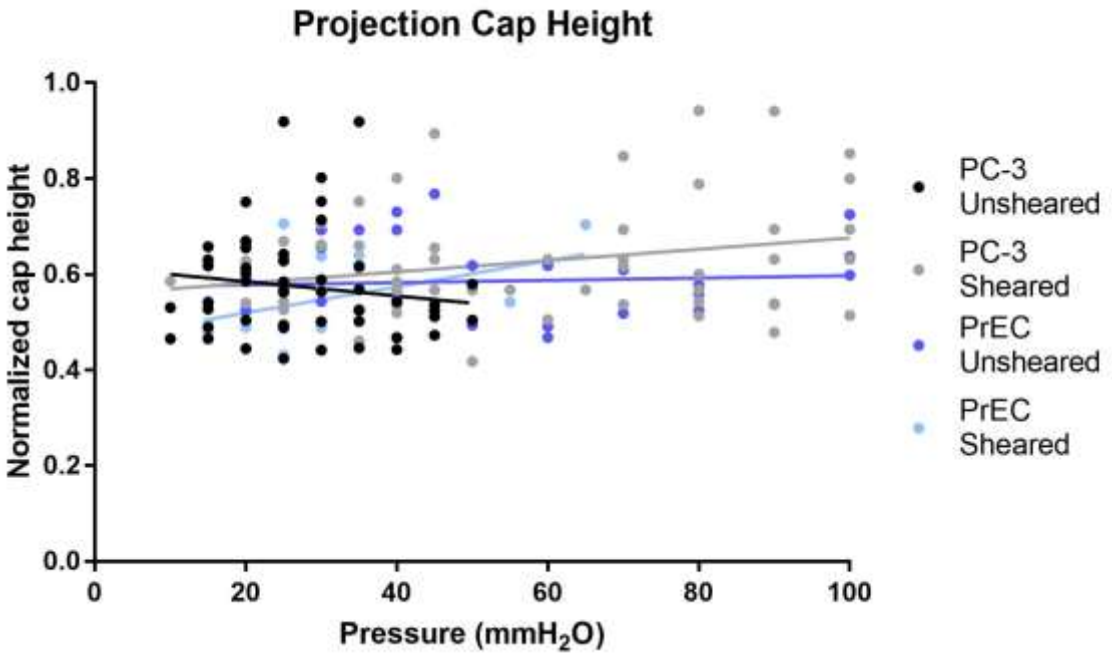

Figure 27: Projection cap heights for cells in each experimental group at the pressure level applied by MPA. Lines represent linear regression fits for the data.

significantly non-zero, is still very small. There is no evidence to indicate that there is a difference in the shape of the projection cap between PC-3 and PrEC cells.

3.2 MATLAB Stress Analysis

The MATLAB model was applied to many of the cells that ruptured during micropipette aspiration. Some of the recorded images were not of high enough quality to be able to plot points along the membrane edge confidently and precisely; these cells were not included in the MATLAB analysis. The model fitted a 2-piece spline to the imported coordinates, then calculated the circumferential and meridional curvature, principal stresses, and von Mises stress along the membrane curve. Examples of these results are presented in Figure 28, Figure 29, and Figure 30. In Figure 28, the solid markers represent the points placed along the edge of the membrane using ImageJ, and the axes represent a simple cartesian coordinate system. The x-axes in Figure 29 and Figure 30 represent arclength along the spline modeling the axisymmetric membrane. An arclength of zero represents the apex of the curve, and an arclength of one represents the

intersection of the membrane with the pipette wall. There were no clear trends in principal stresses or von Mises stress common to the majority of cells studied. Locations for the maxima and minima of the calculated stresses were quite variable, indicating variation in the local curvature of the splines used to fit the data. There was also no clear correlation between the location of rupture observed during MPA and the location of the maximum stress calculated by the MATLAB model.

In general, the maximum stress along the membrane curve did tend to increase with increased pressure levels, as indicated in Figure 31. This figure represents cells from each experimental group and various pressure levels before rupture. The variability of the calculated stress is higher at higher pressure levels, where fewer cells were analyzed. This trend of increasing stress with increasing pressure was also evident for principal stress T_2 and von Mises stress, which is an expected and reasonable result.

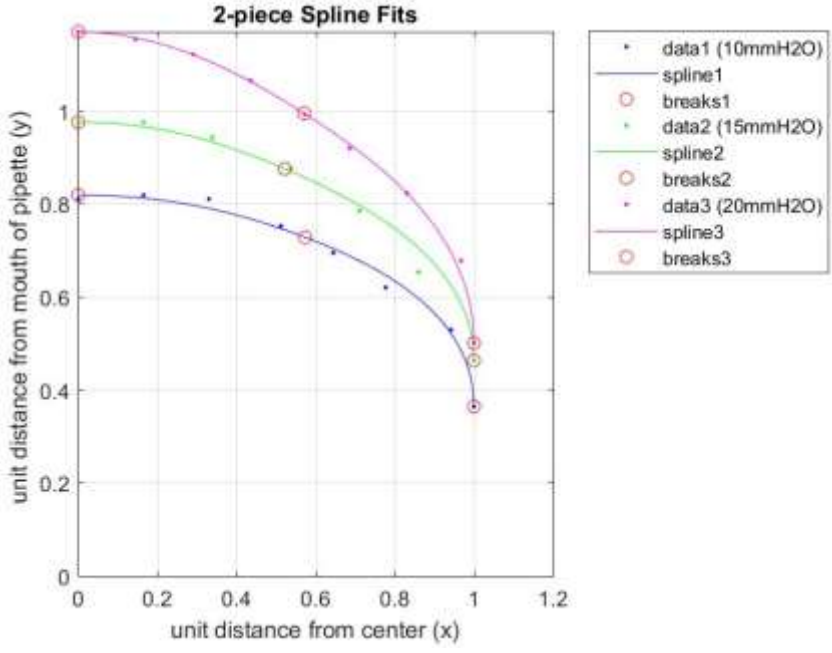

Figure 28: 2-Piece splines fitted to imported coordinates by the MATLAB model. Cell was an unsheared PC-3 that ruptured at 25 mmH_2O.

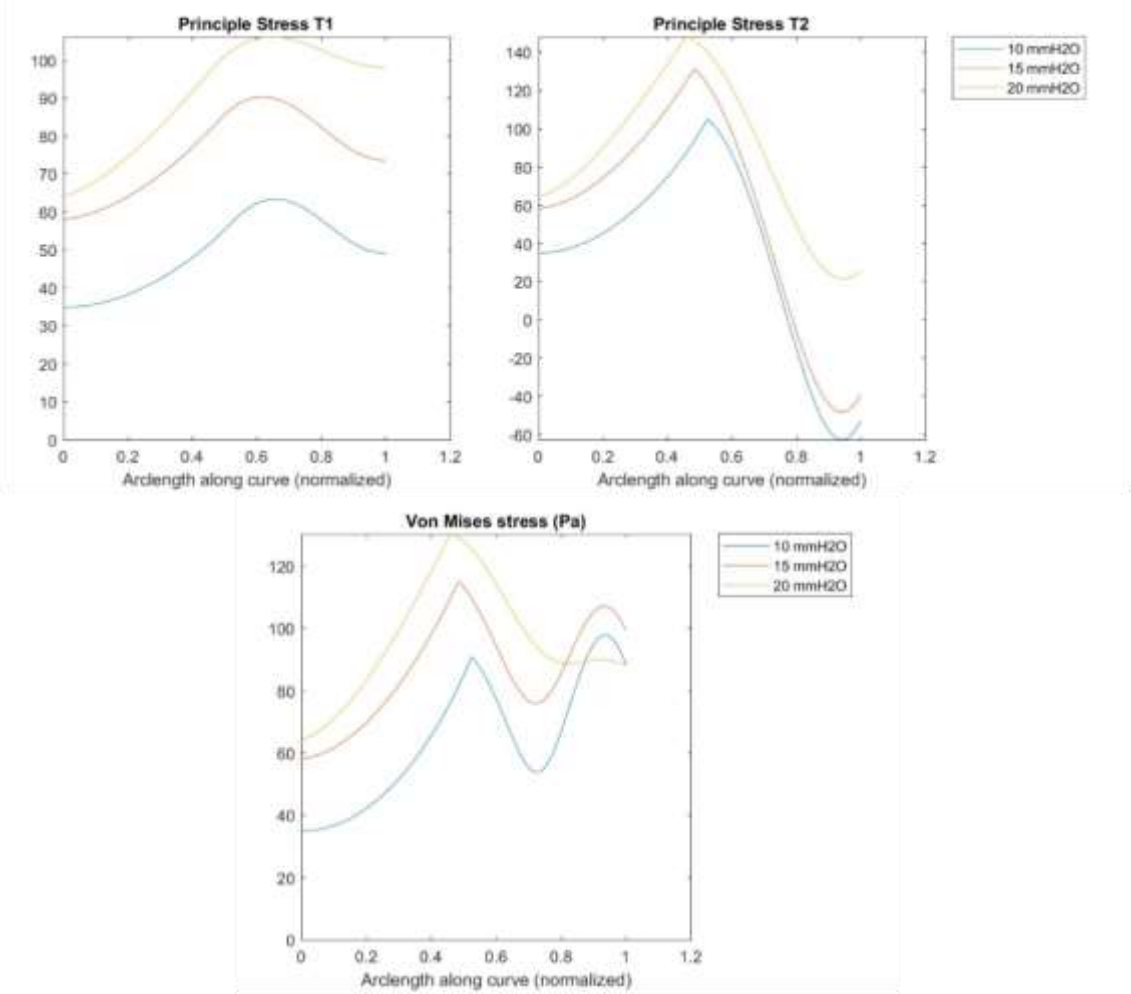

Figure 29: Examples of stresses calculated with the MATLAB model. Cell was an unsheared PC-3 that ruptured at 25 mmH_2O.

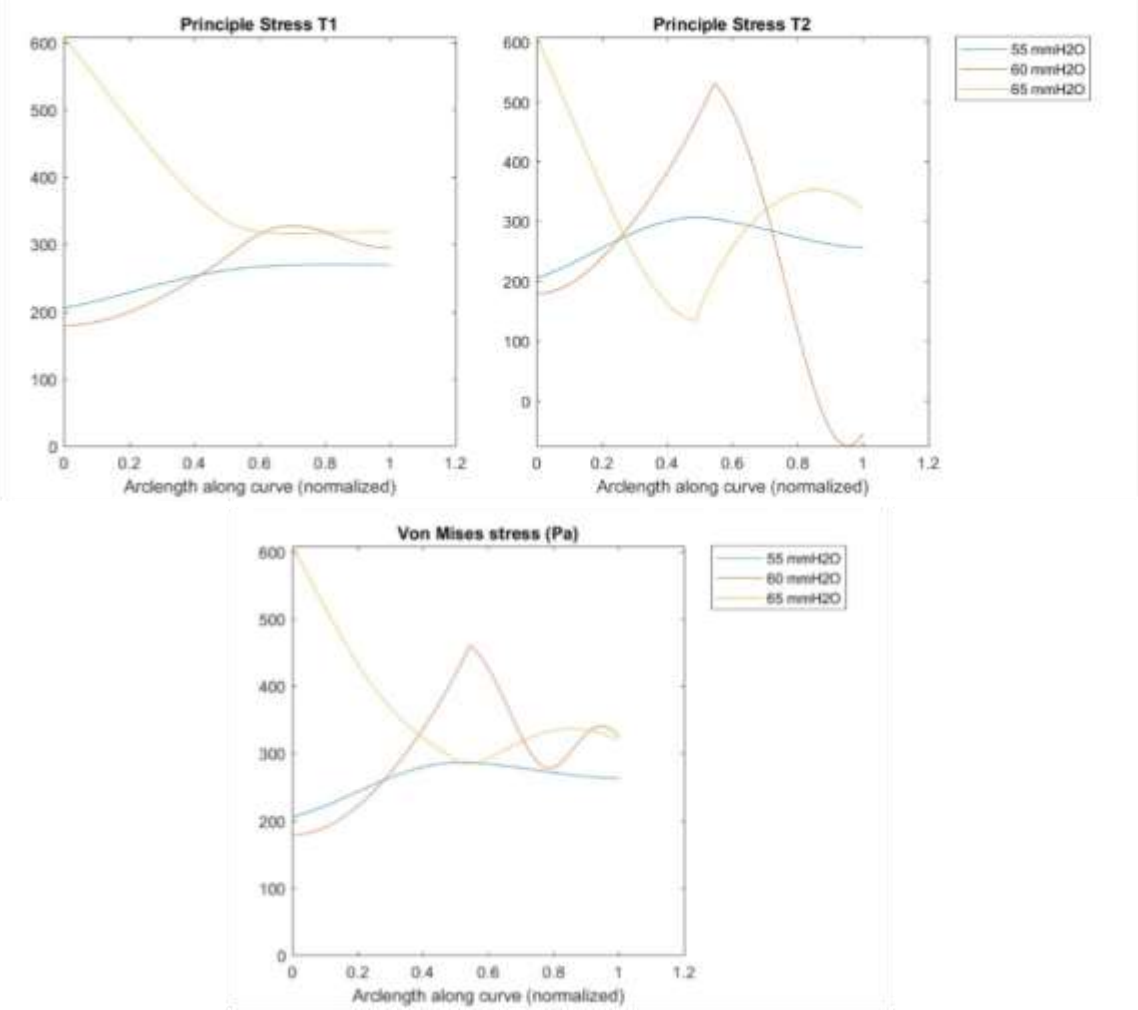

Figure 30: Examples of stresses calculated with the MATLAB model. Cell was a sheared PrEC that ruptured at 70 mmH_2O.

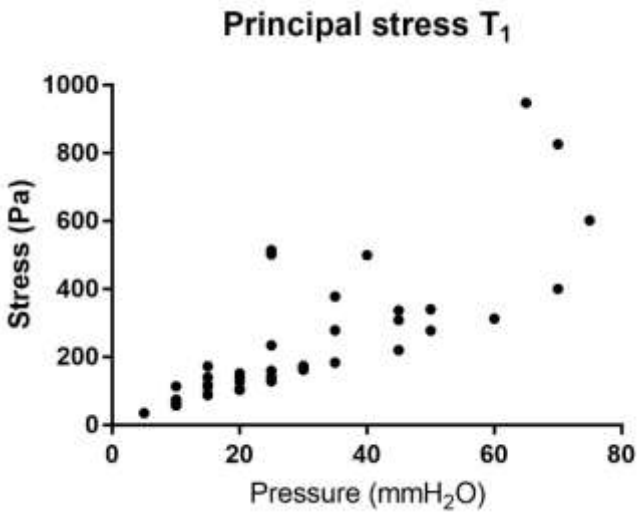

Figure 31: Maximum stress calculated by MATLAB versus pressure level.

3.3 Abaqus Stress Validation

The Abaqus model was solved for three different pressure levels of one of the unsheared PC-3 cells. Solutions converged within a minute of computation time, and the deformation of the geometry was minimal. Principal stresses and von Mises stress were extracted from the model and plotted alongside the MATLAB results to look for continuity in the trends of the stresses. In some cases, the Abaqus results needed to be scaled up by a factor of 10 or 20 to be able to easily compare the trends. A comparison of the results for the cell at the 10 mmH_2O pressure level is presented in Figure 32, Figure 33, and Figure 34 for principal stress T_1, principal stress T_2, and von Mises stress, respectively.

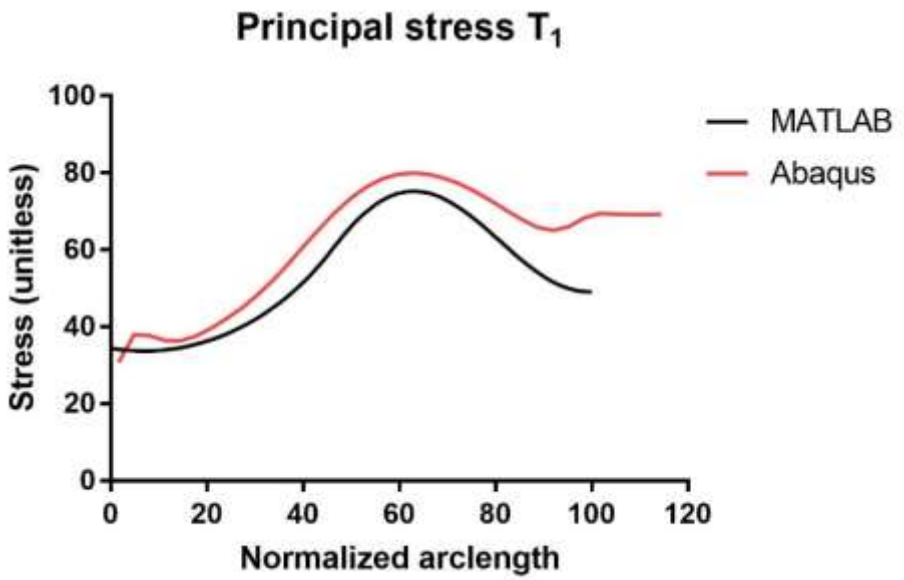

Figure 32: Comparison of results between MATLAB and Abaqus for principal stress T_1. Arclength is normalized to place the intersection between the membrane and the pipette wall at 100.

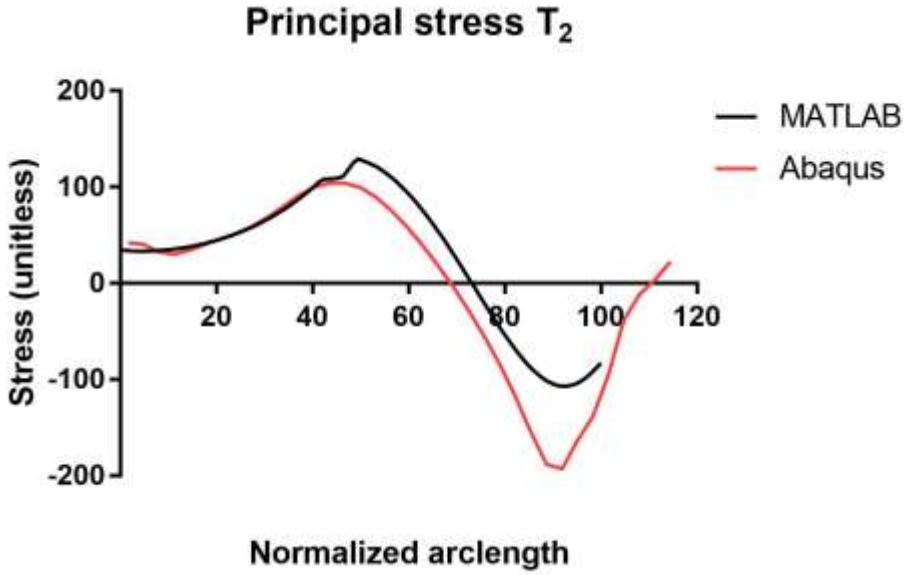

Figure 33: Comparison of results between MATLAB and Abaqus for principal stress T_2. Arclength is normalized to place the intersection between the membrane and the pipette wall at 100.

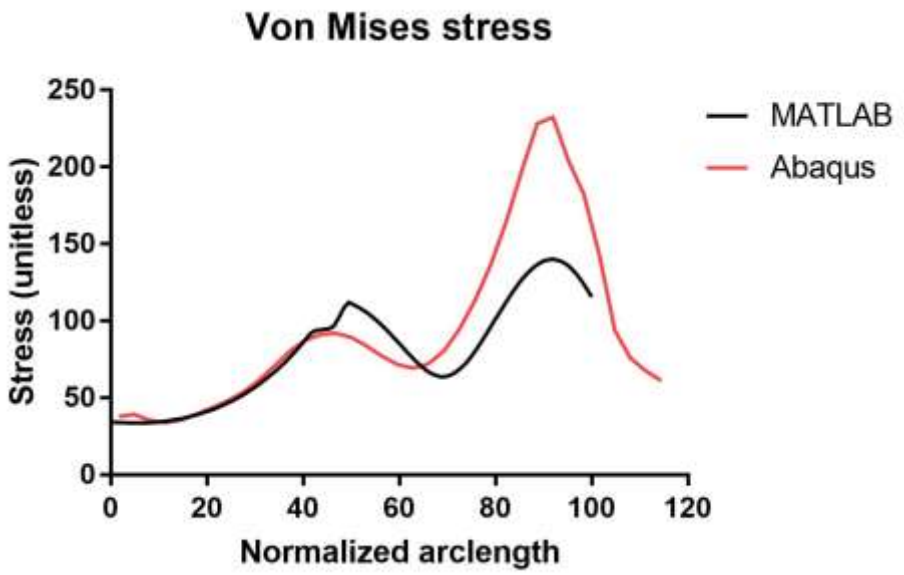

Figure 34: Comparison of results between MATLAB and Abaqus for von Mises stress. Arclength is normalized to place the intersection between the membrane and the pipette wall at 100.

CHAPTER 4: DISCUSSION

4.1 Micropipette Aspiration

There was a significant change in rupture pressure with delay time, but only in cells exposed to shear stress, indicating that the cells have some dynamic mechanical response to the shear stress. When the sheared cells were further grouped by cell type, it was observed that the PrEC cells continued to demonstrate the same decrease in rupture pressure with time. There were too few sheared PC-3 cells measured after 60 minutes delay time to draw any conclusions about the PC-3 group. In general, cells exposed to shear stress could withstand a higher pressure before rupture during micropipette aspiration, but the effect was transient; after 60 minutes delay time following the shear stress assay, the rupture pressure of the cells fell to essentially the same level as that of the unexposed group. This indicates a transient response to shear stress that increases the failure strength of the cell membrane. There is an immediate reaction by the cell to protect itself and mitigate the effects of the shear stress. This also may indicate that the cells that survive shear stress exposure are not just the inherently strong cells, but that there is an adaptive response to shear stress to increase the strength of the membrane, and that this response seems to be short-lived. The mechanism for this increase in membrane strength is not currently known, though it may be hypothesized to be due to a combination of cytoskeletal structures, membrane proteins, and the lipid bilayer itself. There was no change in elastic modulus with time. Any remodeling or repair of the cytoskeleton or extracellular matrix after detachment from the culture dish and the shear stress assay did not significantly contribute to change in cell stiffness within the time frame of the experiments.

There were some significant correlations between elastic modulus or rupture pressure and cell size parameters, as shown in Table 3 and Table 4. Because these correlations were not consistent between the different ways of grouping the data, they were ignored. The effect of cell

size on material properties is unlikely to be a clinically interesting question. It may also be that the significant correlations are false positives, the result of random variation in the MPA data.

4.1.1 Elastic Modulus

Elastic modulus of each experimental group was roughly Gaussian, as demonstrated by the histogram in Figure 22. The average elastic modulus calculated for each experimental group (measured within 60 minutes delay time) was presented in Figure 21. The PC-3 cells' elastic modulus was unchanged by exposure to shear stress. This is in contradiction to the study by Chivukula, which found that PC-3 cells exposed to shear stress became stiffer (Chivukula et al., 2015). The low numbers of cells in the PrEC group prevented the detection of a significant difference between the sheared and unsheared groups. However, the sheared PrEC group had a significantly higher elastic modulus compared to both PC-3 groups.

Previous studies (see Table 1) have found that cancer cells have a significantly lower elastic modulus compared to their untransformed counterparts. This was not seen in this study; the average elastic moduli of the unsheared PC-3 and PrEC cells were not significantly different. This study also found a trend toward increasing elastic modulus with shear stress exposure for the PrEC group, which was not seen in the Chivukula study (Chivukula et al., 2015). However, the low number of cells in the PrEC experimental group certainly limits the power of the study to detect differences in elastic modulus.

A power analysis may be performed to determine whether the experiments in this study had adequate sample sizes. If the differences in elastic modulus between cell types and shear groups seen by Chivukula represent the true means and standard deviations of the populations, power calculations may be used to determine the minimum sample size for an experiment to be likely to detect that difference (Chivukula et al., 2015). The sample size calculation is presented in Equations 20 and 21:

$$n = 2\left(\frac{Z_{1-\alpha/2} + Z_{1-\beta}}{ES}\right)^2 \qquad (20)$$

$$ES = \frac{|\mu_1 - \mu_2|}{\sigma} \qquad (21)$$

where n is the sample size of each experimental group, Z is a statistical factor that depends on the significance and power levels desired for the calculation, ES is the effect size, μ_i is the mean of an experimental group, and σ is the pooled standard deviation of the groups. To have a 90% chance of finding a significant difference between the elastic modulus of unsheared and sheared PC-3 cells (assuming Chivukula's results represent the true means of the populations), the sample sizes of each group should be at least 11 cells. This calculation uses a significance value (α) of 0.05 and power ($1 - \beta$) of 90%. Using the same parameters with the difference in elastic modulus between unsheared PC-3 and unsheared PrEC cells, the minimum sample size of each group was found to be 10 cells. The sample sizes of the PC-3 groups in this study were adequate, but no difference was found in elastic modulus between the PC-3 groups. The unsheared PrEC group was underpowered in this study; the sample size was too small to have a good chance of detecting a significant difference between the groups. In future studies, the sample size of the PrEC groups should be increased.

4.1.2 Rupture Pressure

Rupture pressure of most of the experimental groups displayed a Gaussian distribution, as seen in Figure 23, with the unsheared PrEC cells exhibiting higher variability. The rupture survival curves between experimental groups, as shown in Figure 24, displayed some interesting differences. There was a significant difference between the survival curves for unsheared PC-3 vs sheared PC-3 cells. After exposure to shear stress, the PC-3 cells showed an adaptive strengthening response and could endure a higher aspiration pressure before rupture. The PrEC cells seemed to exhibit little change in their rupture behavior in response to the shear stress, indicating that the PrEC cells may not have the same adaptive ability to strengthen their

membranes after exposure to shear stress. This behavior is evident in the plot of rupture pressure between experimental groups in Figure 26. There was a significant increase in rupture pressure between the unsheared and sheared PC-3 groups. However, there was no significant difference in rupture pressure between unsheared and sheared PrEC cells. It must be remembered that Figure 26 contains only cells that successfully ruptured during the MPA experiment and that were measured within 60 minutes delay time, which places limits on the representative ability of data.

These findings may indicate a cancer-specific adaptive mechanism to shear stress to decrease the likelihood of a cancer cell rupturing while traveling through the circulatory system. Plenty of cells did lyse during the shear stress assay (the cell survival percentage during the shear stress assay was not quantified in this study); this was indicated by cell fragments observed in the culture medium during MPA. The cancer cells that survived, however, seemed to change the rupture strength of their membranes in response to the treatment. This change in rupture pressure after shear stress exposure was not related to a change in elastic modulus, however, or to the shape or curvature of the projection cap. It is possible that rupture is more dependent on biochemical aspects of the cell membrane than on whole-cell biomechanical properties.

4.1.3 Projection Cap Shape

The height of the projection cap did not exhibit significant differences between any of the experimental groups, comparing both the average projection height across several pressure levels and the projection height immediately preceding rupture. The positive correlation between pressure and projection height for the sheared PC-3 and sheared PrEC cells, shown in Figure 27, indicates that the projection caps of the cells exposed to shear stress tend to become rounder as they are aspirated into the pipette. While significantly non-zero, the slope of this relationship is small enough to be considered clinically insignificant. In any case, there is no evidence to suggest that there is a difference in the shape of the projection cap that may lead to different patterns of rupture between PrEC and PC-3 cells. The shape of the membrane does contribute to stress

distribution, but there seems to be no correlation between cell type and membrane curvature patterns.

4.2 Membrane Stress Analysis

The principal stresses and von Mises stress calculated by the MATLAB code were corroborated by the Abaqus model for direction and relative magnitude of the trends. The two types of models often agreed well. However, there seemed to be no correlation between the location of the maximum stresses calculated by the model and the location of rupture observed during MPA. The accuracy of the MATLAB model was limited by the quality of the images collected during MPA and the simplicity of the stress model. The stress model does not account for bending stresses and assumes axisymmetry. The inconsistency of the trends for stress along the membrane indicated changing curvature between pressure levels and between cells, which may be correlated with rupture behavior or may be the result of poor placement of points along the membrane in ImageJ. Each cell analysis investigated the three pressure levels immediately preceding rupture. If lower pressure levels were also evaluated for stress, patterns might emerge in the curvature change of the projection cap during the MPA experiment. Expanding the analysis to include more cells and more pressure levels may reveal patterns in stress distribution or changes in curvature that are not now evident.

One issue noticed during the MATLAB image processing was the sensitivity of the stress model to small changes in curvature in the fitted spline. The spline function was not overly sensitive to the coordinates of the points along the membrane; in fact, the 2-piece spline sometimes did not capture the curvature adequately for more irregularly-shaped membranes. The use of 3-piece or 4-piece splines often better approximated the membrane curvature, but the curvature of the spline was of necessity much more variable. This variable curvature resulted in wildly irregular and difficult to interpret stress results. For this reason, the simpler 2-piece spline was considered to be the optimal option for the stress model.

The accuracy and consistency of the stress model results may be improved by obtaining better quality images during the MPA experiments. This could be accomplished by using a higher quality microscope or controlling the vibration in the room through a vibration table. Using larger diameter pipettes (and therefore larger cells) also tended to produce clearer images. Finally, an automated tool to place points along the membrane curve or to construct a best-fit spline may introduce less user error or bias and make the stress results more consistent. The creation of an image processing algorithm was not the focus of this study, but may be useful in future investigations.

CHAPTER 5: LIMITATIONS AND FUTURE DIRECTIONS

Further studies investigating the effect of fluid shear stress on cancer cells are needed to confirm the hypothesis that shear stress induces a mechanical response in the rupture strength of the cell membranes. Varying the levels of shear stress, such as in the study by Chivukula, will also be helpful in determining if the change in rupture pressure for cancer cells is a graded response (Chivukula et al., 2015). It must also be confirmed whether there is a difference in elastic modulus between cancer and epithelial prostate cells, which has been previously demonstrated but was not seen in this study. Larger sample sizes for the PrEC groups may provide more conclusive results for these measures. Studies with other cancer cell lines can determine if this behavior generalizes to multiple cancer types. Other experimental variables of interest may include temperature of the sample, time of day, culture medium, or long-term exposure to shear stress.

One assumption to declare in relation to the micropipette aspiration experiment is the observation of membrane rupture. The formation of a bleb on the surface of the aspirated membrane is assumed to be a rupture event, with the cell's membrane splitting open and cell contents spilling out. It is possible that this observation is actually a ballooning of the cell membrane, similar to a blood vessel aneurysm, in which the membrane stretches but remains intact. In this case, the stresses in the membrane at the point of bleb formation would be representative of the yield stress of the membrane instead of the failure strength.

The biochemical changes taking place in the cancer cells in response to fluid shear stress are currently unknown. Biomechanical studies are useful to identify macroscopic behavioral changes in cells, but their underlying causes are on the molecular level and are more difficult to identify. The mechanism by which cancer cells resist rupture after exposure to shear stress may be biochemical in nature; if this mechanism can be disrupted, a treatment to reduce the metastatic potential of tumor cells may be created. Prevention of metastasis would be an enormous step

forward for cancer treatment; most metastasis-prevention strategies are still in research and trial phases.

Further refinement of the computational model for membrane curvature and stress would also be helpful to determine true membrane stresses and to relate stress to rupture location along the membrane. It may improve the consistency of the results to create an image processing tool to automatically identify points along the membrane curve. This would remove some of the human error in manually determining coordinates using ImageJ. This would require the creation of image processing and edge detection tools, which was not the focus of this project. Modeling the entire membrane, rather than assuming axisymmetry, would improve the accuracy of the results; however, this would require the use of different and more complicated analytical models for curvature and stress. This would dramatically increase the complexity and computation time of the model.

BIBLIOGRAPHY

Barnes, J. M., Nauseef, J. T., & Henry, M. D. (2012). Resistance to fluid shear stress is a conserved biophysical property of malignant cells. *PLoS One, 7*(12), e50973. doi:10.1371/journal.pone.0050973

Biro, M., & Maitre, J. L. (2015). Dual pipette aspiration: a unique tool for studying intercellular adhesion. *Methods Cell Biol, 125*, 255-267. doi:10.1016/bs.mcb.2014.10.007

Bronkhorst, P. J. H., Streekstra, G. J., Grimbergen, J., Nijhof, E. J., Sixma, J. J., & Brakenhoff, G. J. (1995). A new method to study shape recovery of red blood cells using multiple optical trapping. *Biophys J, 69*(5), 1666-1673.

Butt, H. J., Cappella, B., & Kappl, M. (2005). Force measurements with the atomic force microscope: Technique, interpretation and applications. *Surface Science Reports, 59*(1-6), 1-152. doi:10.1016/j.surfrep.2005.08.003

Cameron, M. D., Schmidt, E. E., Kerkvliet, N., Nadkarni, K. V., Morris, V. L., Groom, A. C., . . . MacDonald, I. C. (2000). Temporal Progression of Metastasis in Lung: Cell Survival, Dormancy, and Location Dependence of Metastatic Inefficiency. *American Association for Cancer Research, 60*(9), 2541–2546.

Chambers, A. F., Naumov, G. N., Vantyghem, S. A., & Tuck, A. B. (2000). Molecular biology of breast cancer metastasis: Clinical implications of experimental studies on metastatic inefficiency. *Breast Cancer Res, 2*(6), 400–407. doi:10.1186/bcr86

Chen, K., Li, D., Jiang, Y. H., Yao, W. J., Wang, X. J., Wei, X. C., . . . Chien, S. (2004). Influence of expressed TRAIL on biophysical properties of the human leukemic cell line Jurkat. *Cell Research, 14*(2), 161–168. doi:10.1038/sj.cr.7290216

Chien, S., Sung, K. L., Skalak, R., Usami, S., & Tozeren, A. (1978). Theoretical and experimental studies on viscoelastic properties of erythrocyte membrane. *Biophys J, 24*(2), 463-487. doi:10.1016/S0006-3495(78)85395-8

Chivukula, V. K., Krog, B. L., Nauseef, J. T., Henry, M. D., & Vigmostad, S. C. (2015). Alterations in cancer cell mechanical properties after fluid shear stress exposure: a micropipette aspiration study. *Cell Health Cytoskelet, 7*, 25-35. doi:10.2147/CHC.S71852

Dholakia, K., & Reece, P. (2006). Optical micromanipulation takes hold. *Nano Today, 1*(1), 18-27. doi:10.1016/s1748-0132(06)70019-6

Efremov, Y. M., Dokrunova, A. A., Efremenko, A. V., Kirpichnikov, M. P., Shaitan, K. V., & Sokolova, O. S. (2015). Distinct impact of targeted actin cytoskeleton reorganization on mechanical properties of normal and malignant cells. *Biochim Biophys Acta, 1853*(11 Pt B), 3117-3125. doi:10.1016/j.bbamcr.2015.05.008

Evans, E. A. (1973). New Membrane Concept Applied to the Analysis of Fluid Shear- and Micropipette-Deformed Red Blood Cells. *Biophys J, 13*(9), 941–954.

Evans, E. A., Yeung, A. (1989). Apparent viscosity and cortical tension of blood granulocytes determined by micropipette aspiration. *Biophys J, 56*(1), 151-160. doi:10.1016/S0006-3495(89)82660-8

Faria, E. C., Ma, N., Gazi, E., Gardner, P., Brown, M., Clarke, N. W., & Snook, R. D. (2008). Measurement of elastic properties of prostate cancer cells using AFM. *Analyst, 133*(11), 1498-1500. doi:10.1039/b803355b

Fidler, I. J. (1970). Metastasis: Quantitative Analysis of Distribution and Fate of Tumor Emboli Labeled With 125I-5-Iodo-2′ -deoxyuridine. *Journal of the National Cancer Institute, 45*(4), 773–782. doi:10.1093/jnci/45.4.773

Fielden, M. (Producer). (2017). AFM Principle. Retrieved from https://www.aphys.kth.se/polopoly_fs/1.672822!/image/AFMprinciple2.jpg

Forouzanfar, M. H., Afshin, A., Alexander, L. T., Anderson, H. R., Bhutta, Z. A., Biryukov, S., . . . Murray, C. J. L. (2016). Global, regional, and national comparative risk assessment of 79 behavioural, environmental and occupational, and metabolic risks or clusters of risks, 1990–2015: a systematic analysis for the Global Burden of Disease Study 2015. *Lancet, 388*(10053), 1659–1724. doi:10.1016/S0140-6736(16)31679-8

Gossett, D. R., Tse, H. T., Lee, S. A., Ying, Y., Lindgren, A. G., Yang, O. O., . . . Di Carlo, D. (2012). Hydrodynamic stretching of single cells for large population mechanical phenotyping. *Proc Natl Acad Sci U S A, 109*(20), 7630-7635. doi:10.1073/pnas.1200107109

Guck, J., Schinkinger, S., Lincoln, B., Wottawah, F., Ebert, S., Romeyke, M., . . . Bilby, C. (2005). Optical deformability as an inherent cell marker for testing malignant transformation and metastatic competence. *Biophys J, 88*(5), 3689-3698. doi:10.1529/biophysj.104.045476

Guo, Q., Park, S., & Ma, H. (2012). Microfluidic micropipette aspiration for measuring the deformability of single cells. *Lab Chip, 12*(15), 2687-2695. doi:10.1039/c2lc40205j

Henon, S., Lenormand, G., Richert, A., & Gallet, F. (1999). A new determination of the shear modulus of the human erythrocyte membrane using optical tweezers. *Biophys J, 76*(2), 1145–1151. doi:10.1016/S0006-3495(99)77279-6

Hochmuth, R. M. (2000). Micropipette aspiration of living cells. *J Biomech, 33*(1), 15-22. doi:10.1016/S0021-9290(99)00175-X

Hochmuth, R. M., Mohandas, N., & Blackshear Jr., P. L. (1973). Measurement of the elastic modulus for red cell membrane using a fluid mechanical technique. *Biophys J, 13*(8), 747-762. doi:10.1016/S0006-3495(73)86021-7

Hochmuth, R. M., Ting-Beall, H. P., Beaty, B. B., Needham, D., & Tran-Son-Tay, R. (1993). Viscosity of passive human neutrophils undergoing small deformations. *Biophys J, 64*(5), 1596-1601. doi:10.1016/S0006-3495(93)81530-3

Hogan, B., Babataheri, A., Hwang, Y., Barakat, A. I., & Husson, J. (2015). Characterizing cell adhesion by using micropipette aspiration. *Biophys J, 109*(2), 209-219. doi:10.1016/j.bpj.2015.06.015

Huang, S., Bow, H., Diez-Silva, M., & Han, J. (2011). *Applying a microfluidic 'deformability cytometry' to measure stiffness of malaria-infected red blood cells at body and febrile temperatures.*

Jones, W. R., Ting-Beall, H. P., Lee, G. M., Kelley, S. S., Hochmuth, R. M., Guilak, F. (1999). Alterations in the Young's modulus and volumetric properties of chondrocytes isolated

from normal and osteoarthritic human cartilage. *J Biomech, 32*(2), 119-127. doi:10.1016/S0021-9290(98)00166-3

Koop, S., MacDonald, I. C., Luzzi, K., Schmidt, E. E., Morris, V. L., Grattan, M., . . . Groom, A. C. (1995). Fate of Melanoma Cells Entering the Microcirculation: Over 80% Survive and Extravasate. *American Association for Cancer Research, 55*(12), 2520-2523.

Lam, J., Herant, M., Dembo, M., & Heinrich, V. (2009). Baseline mechanical characterization of J774 macrophages. *Biophys J, 96*(1), 248-254. doi:10.1529/biophysj.108.139154

Lange, J. R., Steinwachs, J., Kolb, T., Lautscham, L. A., Harder, I., Whyte, G., & Fabry, B. (2015). Microconstriction arrays for high-throughput quantitative measurements of cell mechanical properties. *Biophys J, 109*(1), 26-34. doi:10.1016/j.bpj.2015.05.029

LBM-7 Manual Manipulator. (2015). Retrieved from http://www.scientifica.uk.com/downloads/public/LBM-7-V1.1-Webrez.pdf

Lekka, M. (2016). Discrimination Between Normal and Cancerous Cells Using AFM. *Bionanoscience, 6*(1), 65-80. doi:10.1007/s12668-016-0191-3

Lekka, M., Gil, D., Pogoda, K., Dulinska-Litewka, J., Jach, R., Gostek, J., . . . Laidler, P. (2012). Cancer cell detection in tissue sections using AFM. *Arch Biochem Biophys, 518*(2), 151-156. doi:10.1016/j.abb.2011.12.013

Lekka, M., Laidler, P., Gil, D., Lekki, J., Stachura, Z., & Hrynkiewicz, A. Z. (1999). Elasticity of normal and cancerous human bladder cells studied by scanning force microscopy. *European Biophysics Journal, 28*(4), 312-316. doi:10.1007/s002490050213

Lim, C. T., Dao, M., Suresh, S., Sow, C. H., & Chew, K. T. (2004). Large deformation of living cells using laser traps. *Acta Materialia, 52*(7), 1837-1845. doi:10.1016/j.actamat.2003.12.028

Lundgren, J. (2011). splinefit.

Luzzi, K. J., MacDonald, I. C., Schmidt, E. E., Kerkvliet, N., Morris, V. L., Chambers, A. F., & Groom, A. C. (1998). Multistep Nature of Metastatic Inefficiency: Dormancy of Solitary Cells after Successful Extravasation and Limited Survival of Early Micrometastases. *Am J Pathol., 153*(3), 865–873. doi:10.1016/S0002-9440(10)65628-3

MacDonald, I. C., Groom, A. C., & Chambers, A. F. (2002). Cancer spread and micrometastasis development: quantitative approaches for in vivo models. *Bioessays, 24*(10), 885-893. doi:10.1002/bies.10156

MacKay J.L., K. S. (2012). Measuring the Elastic Properties of Living Cells with Atomic Force Microscopy Indentation. In R. J. Taatjes D. (Ed.), *Cell Imaging Techniques. Methods in Molecular Biology (Methods and Protocols)* (Vol. 931). Totowa, NJ: Humana Press.

MF-900 Microforge. (2018). Retrieved from http://products.narishige-group.com/individual/MF-900/MF-900.jpg

Mietke, A., Otto, O., Girardo, S., Rosendahl, P., Taubenberger, A., Golfier, S., . . . Fischer-Friedrich, E. (2015). Extracting Cell Stiffness from Real-Time Deformability Cytometry: Theory and Experiment. *Biophys J, 109*(10), 2023-2036. doi:10.1016/j.bpj.2015.09.006

Mitchell, M. J., Denais, C., Chan, M. F., Wang, Z., Lammerding, J., & King, M. R. (2015). Lamin A/C deficiency reduces circulating tumor cell resistance to fluid shear stress. *Am J Physiol Cell Physiol, 309*(11), C736–C746. doi:10.1152/ajpcell.00050.2015

Mitchison, J. M., & Swann, M. M. (1954). The mechanical properties of the cell surface. I. The cell elastimeter. *Journal of Experimental Biology, 31*(3), 443-460.

Mofrad, M. R. K., & Kamm, R. D. (2006). *Cytoskeletal Mechanics: Models and Measurements in Cell Mechanics*: Cambridge University Press.

Neuman, K. C., & Block, S. M. (2004). Optical trapping. *Rev Sci Instrum, 75*(9), 2787–2809. doi:10.1063/1.1785844

Nikon DIAPHOT-300 Research-Grade Biotech Inverted Microscope. (2015). Retrieved from http://www.welltechinc.com/userimages/WELL2677_1_NIKON%20Diaphot-300%20Inverted%201.jpg

Nyberg, K. D., Hu, K. H., Kleinman, S. H., Khismatullin, D. B., Butte, M. J., & Rowat, A. C. (2017). Quantitative Deformability Cytometry: Rapid, Calibrated Measurements of Cell Mechanical Properties. *Biophys J, 113*(7), 1574-1584. doi:10.1016/j.bpj.2017.06.073

P-30 Micropipette Puller Operation Manual. (2013). In: Sutter Instrument Company.

P-30 Vertical Micropipette Puller. (2012). Retrieved from https://www.sutter.com/productSM/p30.jpg

Ramos, J. R., Pabijan, J., Garcia, R., & Lekka, M. (2014). The softening of human bladder cancer cells happens at an early stage of the malignancy process. *Beilstein J Nanotechnol, 5*, 447-457. doi:10.3762/bjnano.5.52

Regmi, S., Fu, A., & Luo, K. Q. (2017). High Shear Stresses under Exercise Condition Destroy Circulating Tumor Cells in a Microfluidic System. *Scientific Reports, 7*(39975). doi:10.1038/srep39975

Standard Infuse/Withdraw PHD ULTRA™ Syringe Pumps. (2018). Retrieved from https://www.harvardapparatus.com/media/catalog/product/cache/5/thumbnail/300x300/9df78eab33525d08d6e5fb8d27136e95/7/0/703005_703007_1_1.jpg

Stingray F-080. Retrieved from https://www.alliedvision.com/en/products/cameras/detail/Stingray/F-080/action/pdf.html

Suresh, S. (2007). Biomechanics and biophysics of cancer cells. *Acta Materialia, 55*(12), 3989-4014. doi:10.1016/j.actamat.2007.04.022

Theret, D. P., Levesque, M. J., Sato, M., Nerem, R. M., & Wheeler, L. T. (1988). Application of a homogeneous half-space model in the analysis of endothelial cell. *J Biomech Eng, 110*(3), 190-199. doi:10.1115/1.3108430

United States Cancer Statistics: 1999-2014 Incidence and Mortality Web-based Report. (2017). Retrieved from https://nccd.cdc.gov/uscs/toptencancers.aspx

Weiss, L., Dimitrov, D. S., & Angelova, M. (1985). The hemodynamic destruction of intravascular cancer cells in relation to myocardial metastasis. *Proc Natl Acad Sci USA, 82*(17), 5737-5741.

Weiss, L., Orr, F. W., & Honn, K. V. (1989). Interactions between cancer cells and the microvasculature: a rate-regulator for metastasis. *Clinical & Experimental Metastasis, 7*(2), 127–167. doi:10.1007/BF01787020

WHO. (2018). Cancer Fact Sheet. Retrieved from http://www.who.int/mediacentre/factsheets/fs297/en/

Wu, Y. (2017). *Experimental and Numerical Study on Failure Strength of Aspirated Cell Membrane.* (Master of Science), University of Iowa,

Yousafzai, M. S. (2016). *Cancer cell mechanics and cell microenvironment: An optical tweezers study.* (PhD), University of Trieste,

Zhang, G., Long, M., Wu, Z.-Z., & Yu, W.-Q. (2002). Mechanical properties of hepatocellular carcinoma cells. *World J Gastroenterol, 8*(2), 243-246. doi:10.3748/wjg.v8.i2.243

Zhang, H., & Liu, K. K. (2008). Optical tweezers for single cells. *J R Soc Interface, 5*(24), 671-690. doi:10.1098/rsif.2008.0052

APPENDIX

Table A.1: Average elastic modulus for each experimental group.

		Average Elastic Modulus (Pa)	n
PC-3	**Unsheared**	33.40	23
	Sheared	33.85	25
PrEC	**Unsheared**	38.52	5
	Sheared	59.88	7

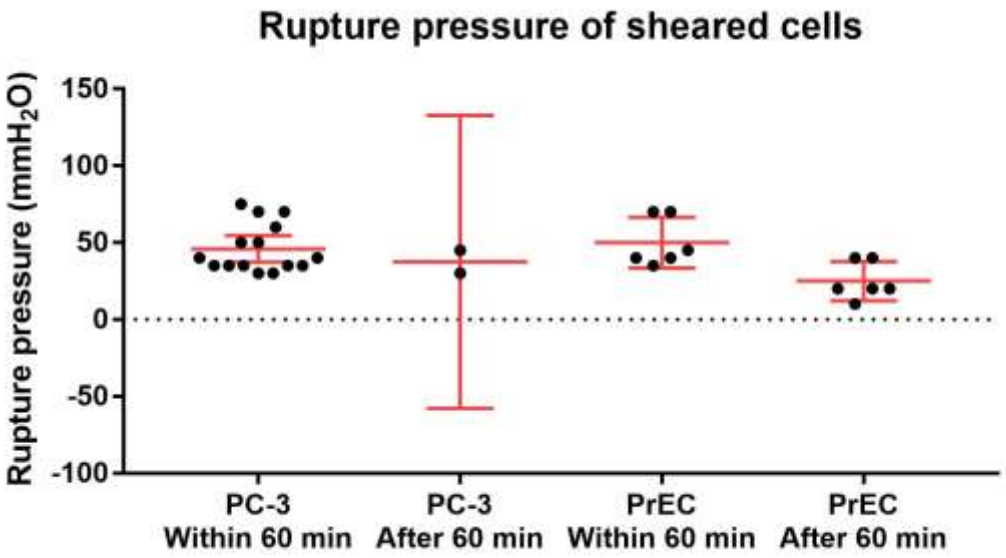

Figure A.1: Rupture pressure of sheared cells measured within 60 minutes delay time and after 60 minutes delay time. Significant difference between PC-3 within 60 minutes and PrEC after 60 minutes ($p = 0.0341$) and between PrEC within 60 minutes and PrEC after 60 minutes ($p = 0.0350$). Error bars represent 95% confidence interval for the mean.

Table A.2: Average and median rupture pressure for each experimental group.

		Rupture Pressure (mmH_2O)			
		Average	**n**	**Median**	**n**
PC-3	**Unsheared**	24.35	23	35	62
	Sheared	46.0	15	70	30
PrEC	**Unsheared**	42.86	7	50	16
	Sheared	50.0	6	40	15

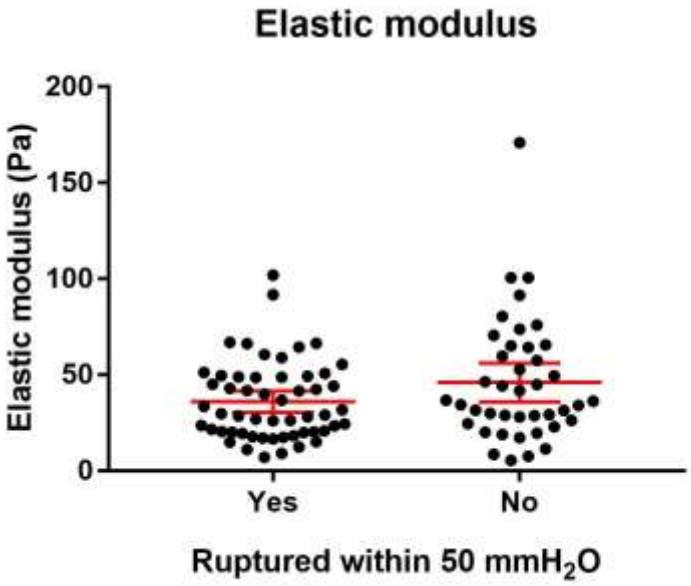

Figure A.2: Elastic modulus data grouped by rupture within 50 mmH_2O. No significant difference in elastic modulus between groups (unpaired t-test, p = 0.0659). Error bars represent 95% confidence interval for the mean.

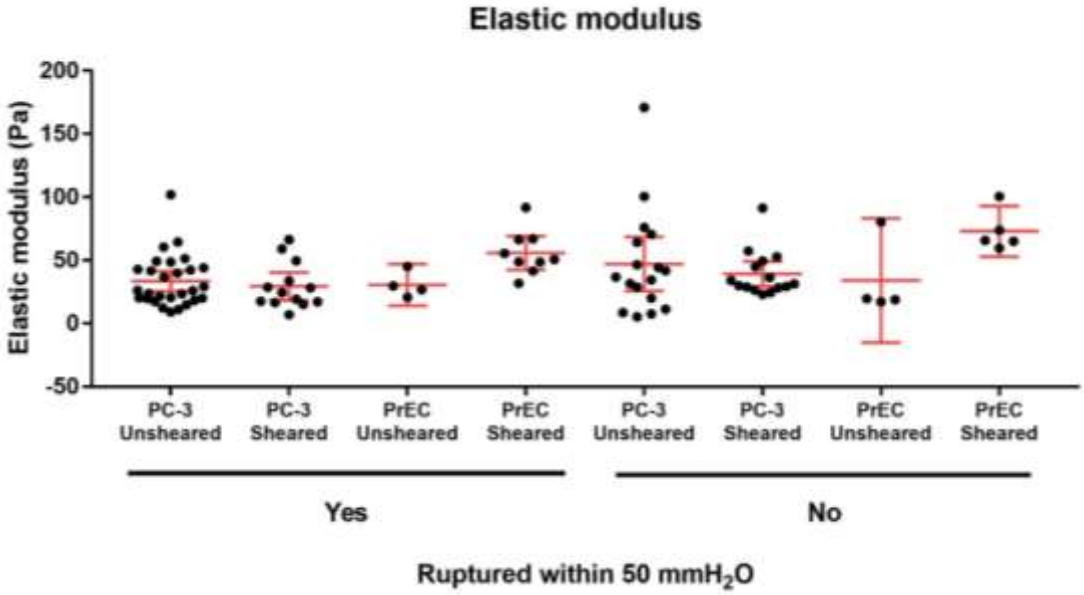

Figure A.3: Elastic modulus data grouped by rupture within 50 mmH_2O, and further divided cell type and shear stress exposure. Significant differences between PC-3 unsheared and ruptured within 50 mmH_2O group and PrEC sheared and unruptured within 50 mmH_2O group (p = 0.0318), and between PC-3 sheared and ruptured within 50 mmH_2O group and PrEC sheared and unruptured within 50 mmH_2O group (p = 0.0270). Error bars represent 95% confidence interval for the mean.

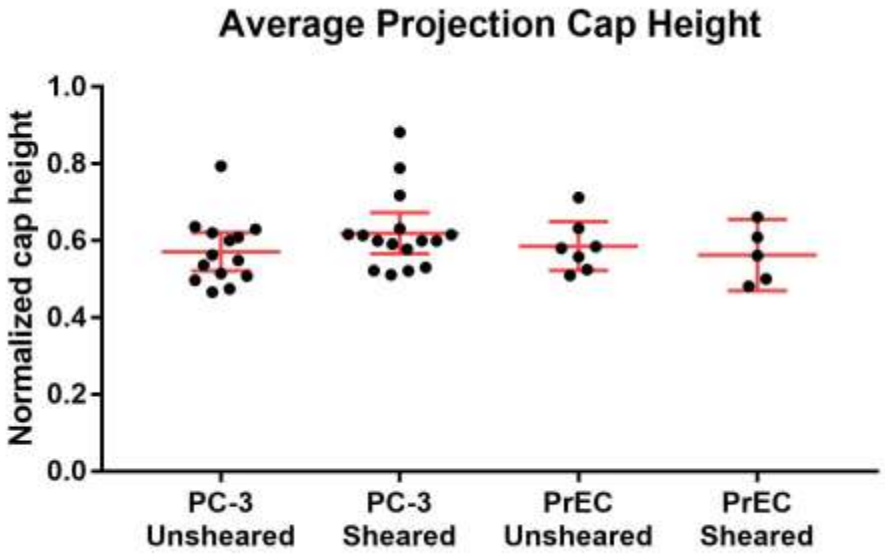

Figure A.4: Average projection cap height. No significant differences between groups. Error bars represent 95% confidence interval for the mean.

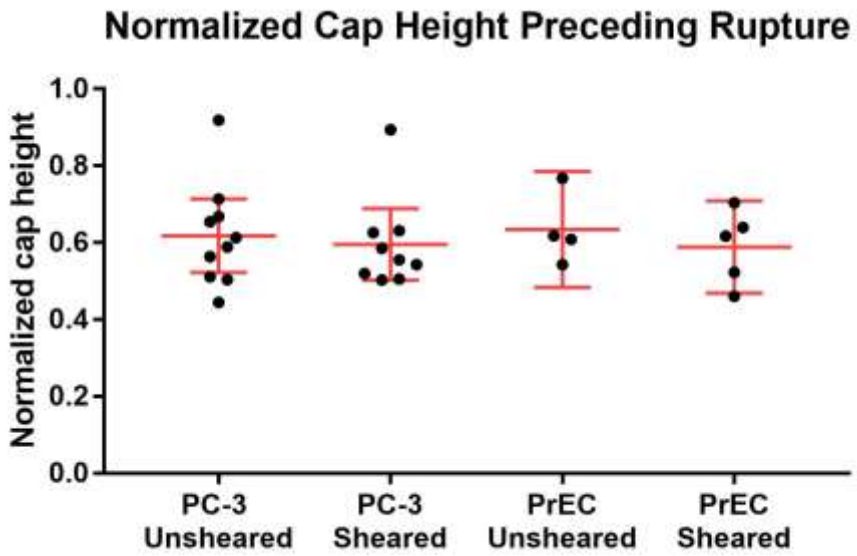

Figure A.5: Projection cap height immediately preceding cell rupture during MPA. No significant differences between groups. Error bars represent 95% confidence interval for the mean.